Journal of Quantitative Spectroscopy & Radiative Transfer 111 (2010) 1043–1064

Contents lists available at ScienceDirect

Journal of Quantitative Spectroscopy & Radiative Transfer

journal homepage: www.elsevier.com/locate/jqsrt

First-principles prediction and partial characterization of the vibrational states of water up to dissociation

Attila G. Császár [a], Edit Mátyus [a], Tamás Szidarovszky [a], Lorenzo Lodi [b], Nikolai F. Zobov [c], Sergei V. Shirin [c], Oleg L. Polyansky [b,c], Jonathan Tennyson [b,*]

[a] Laboratory of Molecular Spectroscopy, Institute of Chemistry, Loránd Eötvös University, P.O. Box 32, H-1518 Budapest 112, Hungary
[b] Department of Physics and Astronomy, University College London, London WC1E 6BT, UK
[c] Institute of Applied Physics, Russian Academy of Sciences, Uljanov Street 46, Nizhny Novgorod 603950, Russia

ARTICLE INFO

Article history:
Received 3 December 2009
Received in revised form
12 February 2010
Accepted 18 February 2010

Keywords:
Water vapor
Transition wavenumbers
Atmospheric physics
Energy levels
Assignation

ABSTRACT

A new, accurate, global, mass-independent, first-principles potential energy surface (PES) is presented for the ground electronic state of the water molecule. The PES is based on 2200 energy points computed at the all-electron aug-cc-pCV6Z IC-MRCI(8,2) level of electronic structure theory and includes the relativistic one-electron mass-velocity and Darwin corrections. For $H_2\,{}^{16}O$, the PES has a dissociation energy of D_0 = 41 109 cm^{-1} and supports 1150 vibrational energy levels up to 41 083 cm^{-1}. The deviation between the computed and the experimentally measured energy levels is below 15 cm^{-1} for all the states with energies less than 39 000 cm^{-1}. Characterization of approximate vibrational quantum numbers is performed using several techniques: energy decomposition, wave function plots, normal mode distribution, expectation values of the squares of internal coordinates, and perturbing the bending part of the PES. Vibrational normal mode labels, though often not physically meaningful, have been assigned to all the states below 26 500 cm^{-1} and to many more above it, including some highly excited stretching states all the way to dissociation. Issues to do with calculating vibrational band intensities for the higher-lying states are discussed.

1. Introduction

The spectroscopy of the water molecule is fundamental to a wide variety of scientific and engineering applications [1]. High-resolution spectra of the water isotopologues have been extensively studied; indeed, several of us are part of an international task group devoted to developing a definitive information system containing water transitions [2]. Computational techniques to study the rotation–vibration states of water up to dissociation for a given potential energy surface (PES), although computationally demanding, have been available for more than a decade [3–5]. However, as noted in Ref. [3], the available potential energy surfaces used in those early calculations were not designed for the high energy region approaching dissociation. The results obtained using those preliminary PESs should therefore be treated with caution. Indeed, as described below, the vibrational states predicted by the earlier studies are, in certain aspects, even qualitatively different from those presented here.

In the last decade or so several *ab initio* [6–8] and semi-theoretical [6,9–12] potential energy surfaces have been produced for the water molecule, driven in large part by the needs of spectroscopic measurements at infrared and visible wavelengths. These potentials have generally aimed at covering spectral regions up to the near-ultraviolet, which is as far as water spectra have so far been probed with one-photon spectroscopy [13,14].

Experimentally, higher regions of the water potential have started to be systematically probed by Rizzo et al. using two- [15,16] and three-photon [16–19] excitation

* Corresponding author.
E-mail address: j.tennyson@ucl.ac.uk (J. Tennyson).

0022-4073/$ - see front matter © 2010 Elsevier Ltd. All rights reserved.
doi:10.1016/j.jqsrt.2010.02.009

schemes. These studies give information on some of the vibrational states of $H_2\,{}^{16}O$ all the way to dissociation and beyond, but are only sensitive to states which are accessed by the excitation scheme chosen. In particular, these experiments probe the lowest local mode pair of stretching states within each polyad plus, in many cases, some bending excitation on top of these. The ability to probe the vibrational levels all the way to dissociation represents a major advance; however, so far only a minority of the states have yielded themselves to observation.

The lack of direct observation of higher vibrational states of water does not necessarily mean that such states are unimportant. For example, recent observations of cometary emission spectra suggest that highly excited vibrational states of water are naturally populated in comets [20], although the mechanism for this remains a matter of speculation.

In this paper we present a complete list of computed bound vibrational energy levels for water almost all the way to dissociation obtained using a new, accurate, global, mass-independent, *ab initio* potential energy surface and variational-like nuclear motion treatments employing exact kinetic energy operators. We also include a discussion of issues related to calculating vibrational band intensities at ultraviolet wavelengths. Finally, we give our best estimates for the (approximate) associated vibrational normal mode quantum numbers where possible.

2. Computational details

2.1. Electronic structure calculations

Our new electronic structure calculations were briefly reported in a communication by Grechko et al. [17]. These calculations used an atom-centered, sextuple-zeta, so-called aug-cc-pCV6Z Gaussian basis set from the correlation-consistent family of Dunning [21]. Unlike the quintuple-zeta and lower sets in this series, this extended basis set is not yet completely standardized. For H, we used the standard aug-cc-pV6Z basis. For O, the aug-cc-pV6Z part of the basis is also standard [22,23] and the "C" (core-correlation) functions are available via EMSL as "cc-pCV6Z(old)" [24]. The basis set employed consists of *s*, *p*, *d*, *f*, *g*, *h* and *i* functions for oxygen and *s*, *p*, *d*, *f*, *g* and *h* functions for hydrogen, yielding for H_2O a total of 562/533 uncontracted/contracted primitive gaussian functions. Note that in previous studies [7,8] on the PES of water we found full augmentation of the basis with diffuse functions (aug) to be of particular importance. No basis set extrapolation to the complete basis set (CBS) limit [25,26] was attempted.

Electron correlation was treated at the internally contracted multireference configuration interaction (IC-MRCI) level [27] with a renormalised Davidson correction (+Q) [28,29]. The calculations were performed using the MOLPRO electronic structure package [30]. Unlike during generation of our earlier CVRQD surface [7,8], employing a valence-only treatment at the IC-MRCI level, here all electrons were directly included in the correlation treatment.

A series of test calculations were performed to study the effect of varying the MRCI reference (complete active) space, which included comparison with small basis (cc-pVDZ) full configuration interaction (FCI) calculations at several geometries, in particular those toward dissociation, and comparisons with a series of single-reference coupled cluster (CC) treatments, up to quadruple excitation (CCSDTQ), at and around equilibrium. The FCI and CC calculations employed the code MRCC [31]. Our final choice for the reference space for the MRCI computations can be designated as (8,2) in C_s point-group symmetry, which means 8 A' and 2 A'' orbitals were chosen to be freely occupied by the 8 valence electrons. This choice extends the (6,2) complete active space used in a number of previous studies [6–8,32]. Calculations were performed at 2 200 geometries which were chosen to thoroughly sample the PES of the ground electronic state of water up to its first dissociation limit. The IC-MRCI(8,2)+Q/aug-cc-pCV6Z energies were augmented by relativistic corrections calculated as the sum of one-electron mass-velocity and Darwin (MVD1) terms [33,34]. These energies were fitted to a flexible functional form [35] suitable for generating a dissociative PES; an electronic version of the resulting surface has been given previously [17].

2.2. Nuclear motion computations

Nuclear motion calculations were performed on our new potential energy surface using several codes developed either in London or in Budapest, all based on exact kinetic energy operators. The masses (in u) adopted in all computations were m_H = 1.007276 and m_O = 15.990526.

An augmented version of the DVR3D program suite [36,37] employing orthogonal Radau coordinates and a discrete variable representation [38,39] of the Hamiltonian was used to obtain the energy values reported in this paper. Calculations were performed using previously optimized [16] spherical-oscillator [40] functions for the radial and Legendre functions for the angular motions (120 and 70 of them, respectively, during the final run). Increasing the size of the final, contracted Hamiltonian matrix from 15 000 to 20 000 changed the VBOs by no more than 0.1 cm^{-1}. These calculations converged energy levels to better than 1 cm^{-1}, with the exception of an even state at about 40 570 cm^{-1} which can tentatively be identified as (0 26 0) and which shows considerable sensitivity to the number of angular grid points used. Convergence of the computed energy levels was checked using the latest variant of the code DOPI3 [41], D2FOPI [42]. DVR3D and D2FOPI agreed to better than 1 cm^{-1} for all the VBOs reported. Altogether 1 150 VBOs are supported by our computations up to 41 083 cm^{-1}. This energy range includes the last observed pair of vibrational state below dissociation; above this the open nature of the PES (see below) should lead to an increasingly diffuse set of vibrational states which we have not attempted to systematically characterize. The last bound state assigned by our present computations of even symmetry is at

41 082.75 cm^{-1}, it is (19 0 0) in normal-mode notation (*vide infra*). The last assigned bound state of odd symmetry, (18 0 1), is at 41 082.78 cm^{-1}.

Approximate vibrational band intensities were calculated using the Eckart frame [43] and an updated version of the code DIPJ0 [36]; as a check parallel transitions intensities were also calculated taking three times the $J=0\rightarrow1$ transition intensity calculated using the code DIPOLE3 [37]. Our calculations initially used the recently developed CVR dipole moment surface (DMS) of water [32]. For vibrational states lying at infrared and visible frequencies, our calculations gave satisfactory agreement with observed band intensities [44]. However, these calculations gave surprisingly strong band intensities above 30 000 cm^{-1}. Calculations with the dipole moment surface of Schwenke and Partridge (SP2000) [45] gave qualitatively the same results but significantly different intensities for individual states. Previous analyses [32,45] have shown that small imperfections in the fits can lead to the calculation of over-intense transitions for bending overtones at visible wavelengths. We suspected that similar effects were causing our calculations to overestimate the vibrational band intensities to higher vibrational states. Tests performed with low-order polynomial fits to the dipole moment surface supported this conjecture.

As a final test we tried the DMS of Gabriel et al. [46]. This surface, which was demonstrated by the authors to give very good results for the vibrational band intensities of low-lying states, retains no terms higher than fourth-order in the fit. We note that the fit of Gabriel et al. is only valid for a rather limited range of nuclear geometries; however, as here we only consider transitions from the vibrational ground state this should not be a problem. This calculation gave significantly lower vibrational band intensities than equivalent calculations using the CVR or SP2000 surfaces, see Fig. 1. Our conclusion from these studies is that it is not possible at present to make secure predictions of the vibrational band intensities, or indeed of the intensity of individual rotation–vibration transitions, going from the ground vibrational state directly to states lying in the ultraviolet.

Vibrational energy levels and wave functions were also determined with the DEWE program system [47,48] to help the assignment of normal mode labels. DEWE is based on the DVR of the Eckart–Watson Hamiltonian [49,50] and allows the exact inclusion of a PES represented in arbitrarily chosen coordinates. The DEWE computations employed a direct-product Hermite-DVR grid with 20 and 75 grid points for the bending and stretching vibrational degrees of freedom, respectively.

2.3. Wave function plots

Generation of the plots corresponding to real wave functions employed a locally developed code [51]. The input to the code is the file with the wave functions obtained with DVR3D for $J=0$. All the 1 150 wave function plots are given as PDF files in the Supplementary Material. The plots of real wave functions contain two-dimensional (2D) cuts of the functions presented in the three usual Radau coordinates, r_1, r_2, and θ. We note that for water Radau coordinates are very close to the more standard bondlength–bondangle coordinates.

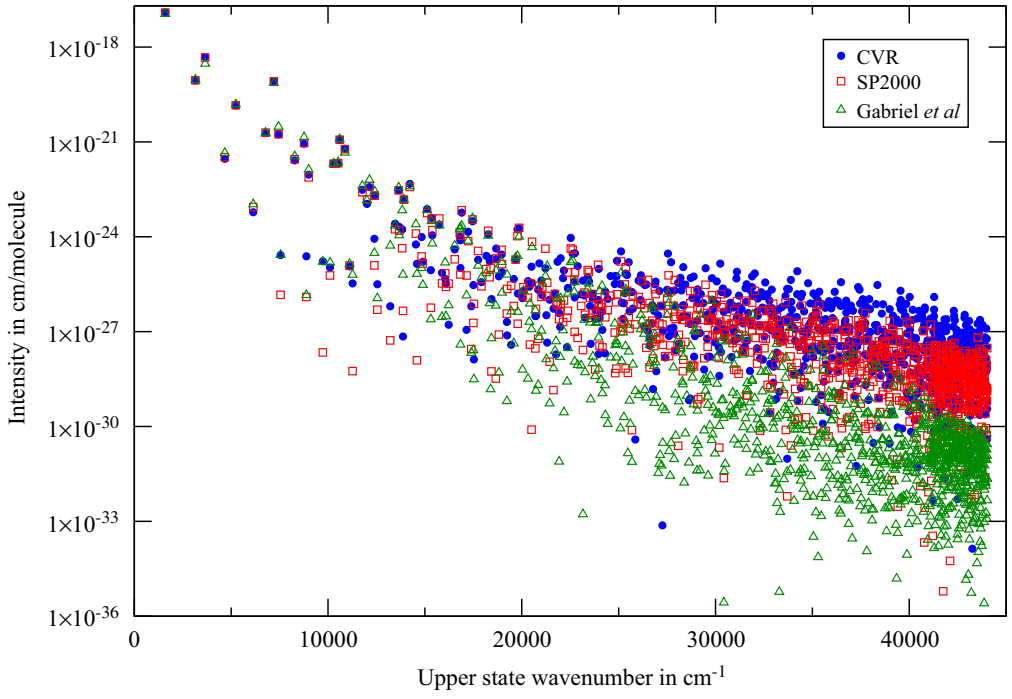

Fig. 1. Vibrational band intensities for even-symmetry H_2O states calculated using three different dipole moment surfaces (DMSs). The plot shows that for transition energies above ≈30 000 cm^{-1} recent DMSs based on high-order polynomial expansions such as CVR and SP2000 considerably overestimate band intensities. See text for details and references.

Wave function plots for selected states are presented in Figs. 2–5. In Figs. 2–5 the positive and negative values are in red and blue, respectively. Change of colors therefore indicates a node in the wavefunction. Each plot also gives a contour corresponding to the classical turning point of the potential at the eigenenergy of the state under consideration. This contour is useful for assessing the chaotic nature of the state: classically chaotic states are ergodic meaning that they sample all available phase space (see Fig. 5). Quantum mechanically an ergodic state would be expected to sample the whole of the available PES [52]. We note that for states near dissociation the potential is in principle open to dissociation, although the molecule has insufficient energy to occupy the OH vibrational ground state and therefore to dissociate. This is a feature of all polyatomic systems and has been found to lead to interesting asymptotic structures in the vibrational states [53].

3. Results

Table 1 presents our calculated vibrational band origins (VBOs) for H_2 ^{16}O up to 25 200 cm^{-1}; where possible, they are compared to available experimental data [16–18,54,55]. It should be noted that as yet transitions to only about 15% of all the VBOs have actually been observed, so the majority of the reported levels represent our predictions for VBOs of water. Table 1 also lists approximate vibrational quantum numbers and information related to several assignment schemes for many of the calculated VBOs. A complete set of VBOs determined in this study are given as Table S1 in the Supplementary Material. Those VBOs lying above 25 200 cm^{-1} for which we could determine approximate normal mode labels are given in Table 2; this table covers all those higher-lying VBOs which have experimental counterparts.

3.1. Quality of the PES

In the past we have advocated the use of the composite focal-point analysis (FPA) approach [25,26,56,57] for the computation of the PESs and DMSs of smaller molecules [7,8,32,58]. There were three reasons for deviating slightly from this approach during this study. First, previous electronic structure studies on the ground-state PES of water [7,8] and on its barrier to linearity [59,60] proved that one must use as large of a Gaussian basis set as possible for treating appropriately the large-amplitude excited bending and stretching motions of water. This limits considerably the accessible choices for the level of electronic structure theory applicable to generate the large number of energy points needed for the surfaces. Second, it turned out that high quality treatment of electron correlation is less important than the choice of the Gaussian basis. Third, by far the most important so-called "small effects" [26] are the core and the MVD1 relativistic energy corrections, covered by the present study in a single computation per energy point. The present PES, when used in a variational nuclear motion computation with exact kinetic energy operators, can reproduce excellently the measured vibrational energy levels up to the dissociation limit. The differences between the computed and the experimental levels can be seen in Fig. 6.

There are a number of salient features of the present PES which are worth discussing. The Born–Oppenheimer equilibrium structure, r_e^{BO}, has r_e(OH)=0.95782 Å and θ_e(HOH) = 104.46°. These values are extremely close to the best available r_e^{BO} estimates, corresponding to the composite CVRQD PES of H_2 ^{16}O [61], namely r_e=0.95785 Å and $\theta_e = 104.50°$. The independent quadratic force constants, in units of aJ $Å^n$ rad^{2-n}, n=0 − 2, corresponding to the global PES are f_{rr} = 8.453, $f_{rr'} = -0.105$, $f_{\theta\theta} = 0.704$, and $f_{r\theta} = 0.257$. These valence coordinate force constants are also very close to those characterizing the CVRQD PES (f_{rr}=8.460, $f_{rr'} = -0.103$, $f_{\theta\theta} = 0.703$, and $f_{r\theta} = 0.258$). These structural and force field parameters have been used, along with the masses, to construct the normal coordinates in DEWE and the normal mode decomposition. Finally, we note that the D_0 dissociation energy of H_2 ^{16}O for the present *ab initio* PES differs from the well-established experimental value, 41 145.94(15) cm^{-1} [19], by only 37 cm^{-1}. This difference comes about as follows. The aug-cc-pCV6Z IC-MRCI+Q(8,2) PES has D_e=43 951 cm^{-1}. The MVD1 correction to this is −50 cm^{-1}. The zero-point vibrational energy (ZPVE) correction for H_2O, corresponding to the present PES, is −4 638.6 cm^{-1} (compare to −4 638.3 cm^{-1} corresponding to the CVRQD PES), while that of OH is +1 847 cm^{-1}.

The results presented above and below and the benchmark *ab initio* calculation of D_0 by Ruscic et al. [62] together with the results of previous studies on water built upon the FPA philosophy can be used to provide pointers on how one could improve the present global potential. There are at least four main "effects" not considered in our computational treatment. First, the aug-cc-pCV6Z basis set used, while very large, carries a basis set incompleteness error (BSIE) due to its finite size and especially to the use of fixed exponents and centers [63]. We estimate that the correction to D_0 due to BSIE may be as much as +80 cm^{-1}. Second, estimation of the correlation energy is based on the IC-MRCI approach which, with respect to full-CI, introduces a noticeable error. As several observations made during this study suggest, this error could be as large as 40–50 cm^{-1}. For example, using the cc-pVDZ basis which permits going to the FCI limit, further away from equilibrium the error of IC-MRCI+Q using the enlarged active space is of the order of 40 cm^{-1}. Third, though scalar relativistic effects, calculated as expectation values of the mass-velocity and one-electron Darwin operators, were included in the calculation, these do not account for all relativistic effects even for the molecule of water [64,65]. Of particular concern when approaching the first dissociation limit, not considered in the present study, is the effect of spin–orbit interaction on D_0. It was reported by Ruscic et al. [62] to be 38 cm^{-1}. Fourth, the electronic structure treatment employed does not go beyond the Born–Oppenheimer separation of nuclear and electronic degrees of freedom. An improvement in the accuracy of the *ab initio* calcula-

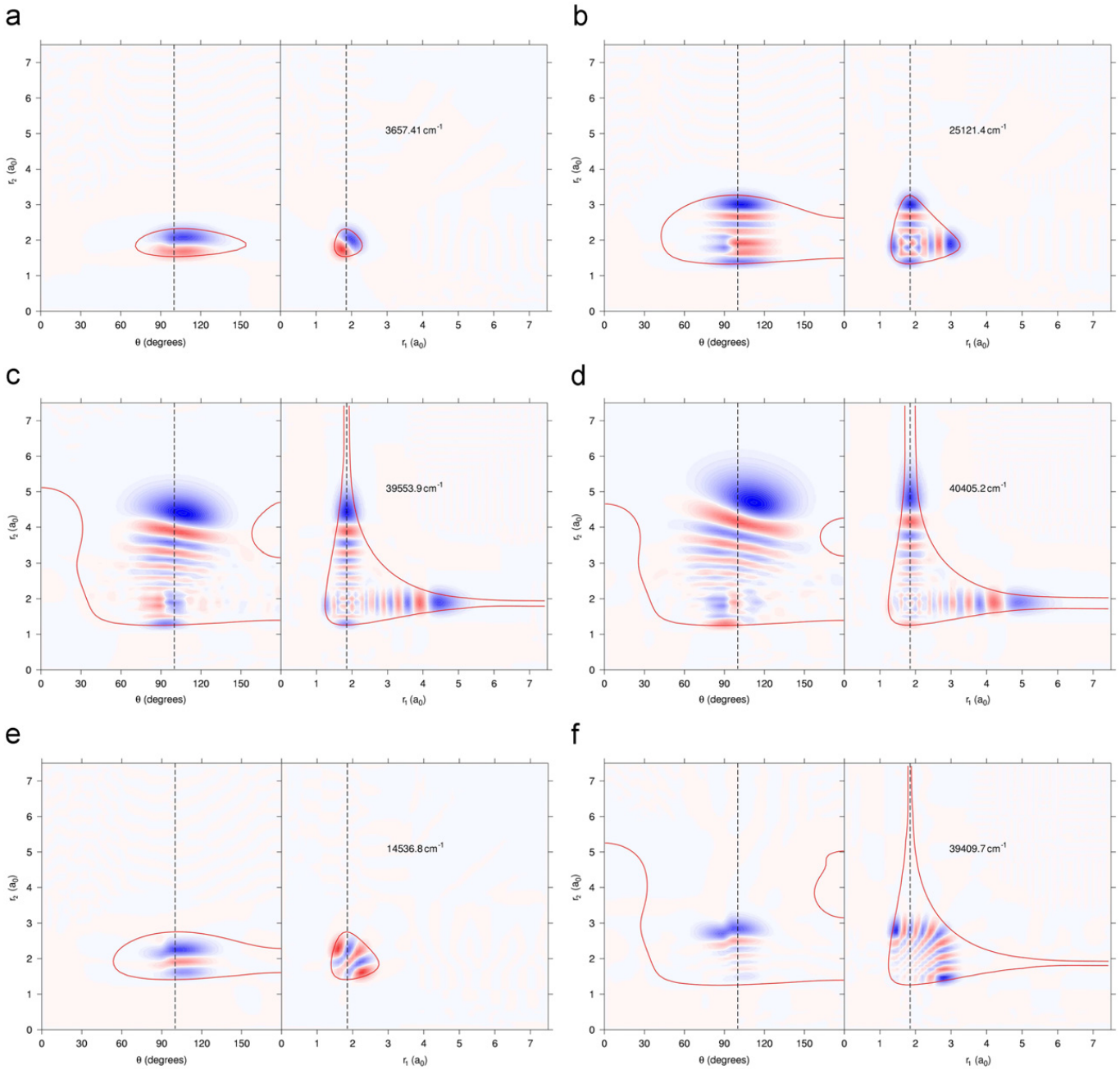

Fig. 2. Plots of real wave functions for selected pure symmetric and antisymmetric stretching states of even symmetry. For symmetric stretches the nodes can be observed along the r_1 and r_2 internal coordinates. For antisymmetric stretches the nodes are along r_1-r_2. Each plot also gives a contour corresponding to the classical turning point of the potential at the eigenenergy of the state under consideration. The plots and thus the states are labelled as $(\nu_1\ \nu_2\ \nu_3)$, for details see the text. (a) (1 0 0), (b) (8 0 0), (c) (16 0 0), (d) (17 0 0), (e) (0 0 4), (f) (0 0 12).

tions could be made by inclusion of adiabatic and non-adiabatic corrections. For example, the adiabatic correction contributes about $+40\,\mathrm{cm}^{-1}$ to the dissociation energy. The non-adiabatic contribution is hard to estimate but we would expect it to partially cancel the adiabatic correction. In summary, even at the very high level of electronic structure theory employed in this study it seems that we are gaining accuracy from a fortuitous cancellation of some of the effects mentioned and not taken into account. Further advance in the *ab initio* computation of the complete set of VBOs for water would benefit only from a joint consideration of all these factors as individual inclusion of any one of them might even make some of our predictions appear worse.

3.2. Vibrational band origins

Some estimates of the accuracy of our first-principles predictions can be made by comparison of the computed VBOs with the observed ones. Fig. 6 shows that not only the differences are small but also the trends are systematic. For the lower-energy VBOs there are clear series corresponding to bending overtones with no

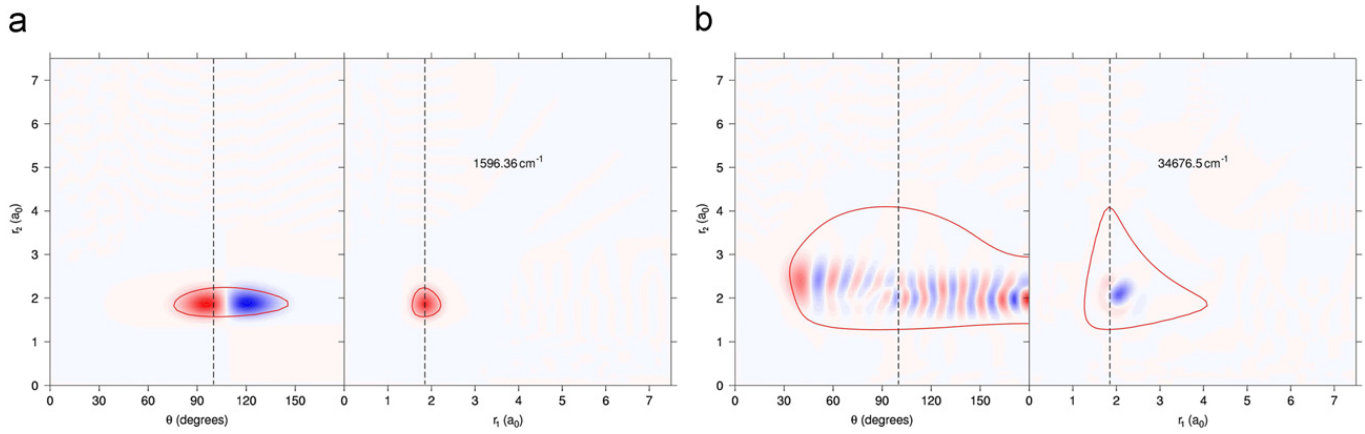

Fig. 3. Wave function plots for pure bending states. For a detailed description see the legend to Fig. 2. (a) (0 1 0), (b) (0 22 0).

stretching excitation, one quanta of stretch (two series), two quanta of stretch (two series) and three quanta of stretch (two series). These series show that the errors increase quite rapidly with increasing bending excitations: it is actually well known that this motion is hard to treat correctly *ab initio* [66,67]. At higher frequencies there are very few observed states with significant bending excitation. In contrast the errors in the calculated pure stretching VBOs remains small, 1 cm^{-1} or less, up to about 25 000 cm^{-1}; above this value the error becomes positive and then, in the last 2000 cm^{-1} below dissociation, sharply negative. At dissociation the error in the highest stretching states, (17 0 0)–(18 0 1), approaches 40 cm^{-1}, the amount our PES underestimates D_0. The systematic nature of these errors suggest that there is scope to improve the calculated VBOs by fitting the PES to the observed levels. Predicted transition frequencies based on the predicted VBOs can be improved either by making manual corrections [68] or by performing a fit to the experimental data starting from our PES.

It can be expected that vibrational band intensities decrease systematically with increasing energy of the VBOs since it is well known that overtone bands become increasingly weaker. However, this decrease is not monotonic with respect to the energy. Instead, some stretching VBOs decrease less rapidly than others as could be anticipated from the fact that direct excitation of states with eight quanta of stretch has already been achieved using cavity ring-down spectroscopy [14].

The absorption of light by water vapor at ultraviolet wavelengths could be of atmospheric importance, particularly at wavelengths below the onset of the main ozone absorptions. The ability to estimate the magnitude of this absorption should be within the scope of our present study but in practice we found that the presently available dipole moment surfaces are not suitable for such calculations. The harmonic model of molecular vibrations suggests that the intensity of a fundamental transition depends principally on the first derivative of the dipole moment at equilibrium taken along the vibrational mode being excited. Within this model, the intensity of the n th overtone then depends on the $(n+1)$th derivative of the dipole surface. What we have found is that the best dipole moment surfaces available for water [32,45] do not give reliable tenth or higher derivatives in the region of equilibrium geometry. Resolving this problem will be the subject of future work. Before leaving this topic we should note that our concern about the use of the available dipole moment surfaces for studying high overtones does not invalidate the transition intensity calculations presented by Grechko et al. [17]. In this work intensities were given for individual rotation–vibration transitions which reached states near the dissociation limit. However, these transitions link states differing by 8 or less quanta of stretch, for which no difficulties have been identified.

3.3. Vibrational state assignments

The variational-type nuclear motion procedures employed in this study are based on the use of rigorous quantum numbers. For the vibrational states of $H_2{}^{16}O$ this means that the states are only distinguished by a single quantum number: the permutational symmetry of the state, which can be viewed as $(-1)^{v_3}$ for states with a normal-mode assignment, where v_3 is the vibrational normal-mode quantum number corresponding to the antisymmetric stretch. Other, approximate vibrational quantum number labels have to be assigned by other means.

Previous calculations [3], which used a different PES, suggested that at energies approaching D_0 the vibrational states of water become highly irregular with little systematic underlying structure. This situation is not promising for assigning approximate vibrational labels. Indeed, there is no guarantee that such labels exist [52], although there are clear rules when they can be considered rigorous [69].

In some contrast to this picture, a previous joint experimental–theoretical study of water spectra up to dissociation [17] observed spectra which were strongly structured with a relatively small number of fairly strong lines. This observation was mirrored by the associated transition intensity calculations. For these states, at least, it proved straightforward to assign vibrational labels [17]

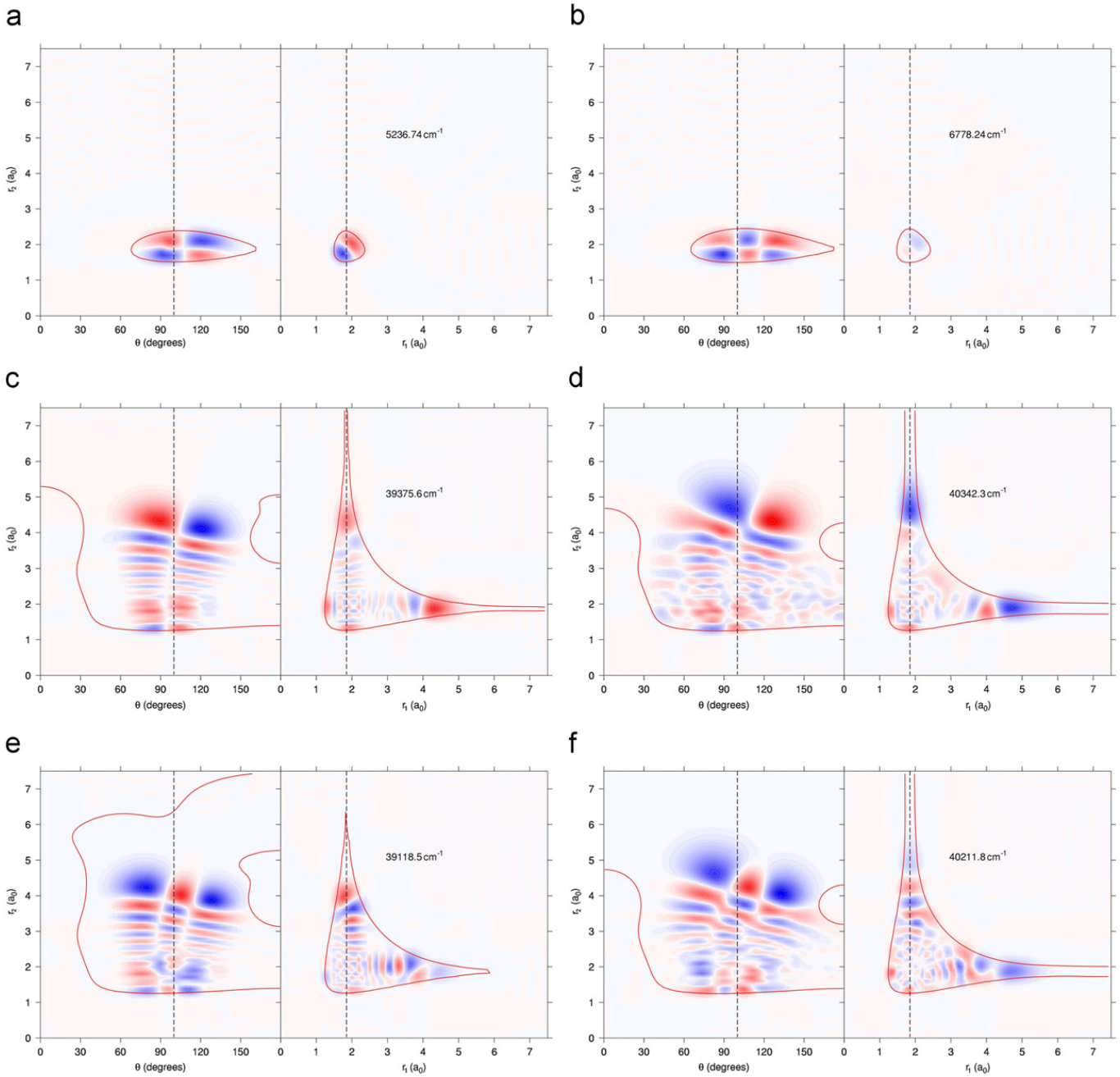

Fig. 4. Wave function plots for stretching states with small bending excitation. For a detailed description see the legend to Fig. 2. (a) (1 1 0), (b) (1 2 0), (c) (15 1 0), (d) (16 1 0), (e) (14 2 0), (f) (15 2 0).

using the PES described here. These results demonstrate that the VBOs given by our PES are at least partially structured. This motivated us to try and find a set of labels for as many vibrational states as possible, extending a previous study of some of the authors [70] employing a different PES.

To make normal mode quantum number assignments, five strategies were investigated.

1. Energy decomposition. The simplest method is to use the energy dependence based on the normal mode quantum numbers. This can be expressed as

$$E(v_1,v_2,v_3) = v_1\nu_1 + v_2\nu_2 + v_3\nu_3, \quad (1)$$

where v_1, v_2, v_3 (v_1 v_2 v_3) and ν_1, ν_2, ν_3 are the vibrational quantum numbers and the vibrational fundamentals for the so-called symmetric stretch, bend, and antisymmetric stretch normal modes, respectively. This method works well up to about 12 000 cm^{-1} and no additional information is required to label the VBOs. We note that at the higher end of this region the stretching motions of water are already much closer described by a local mode rather than a normal mode picture [71]. Above this energy, the density of states increases and there are often several candidates for a given set of vibrational normal mode quantum numbers. Furthermore, as the normal mode decomposition (NMD) analysis presented below

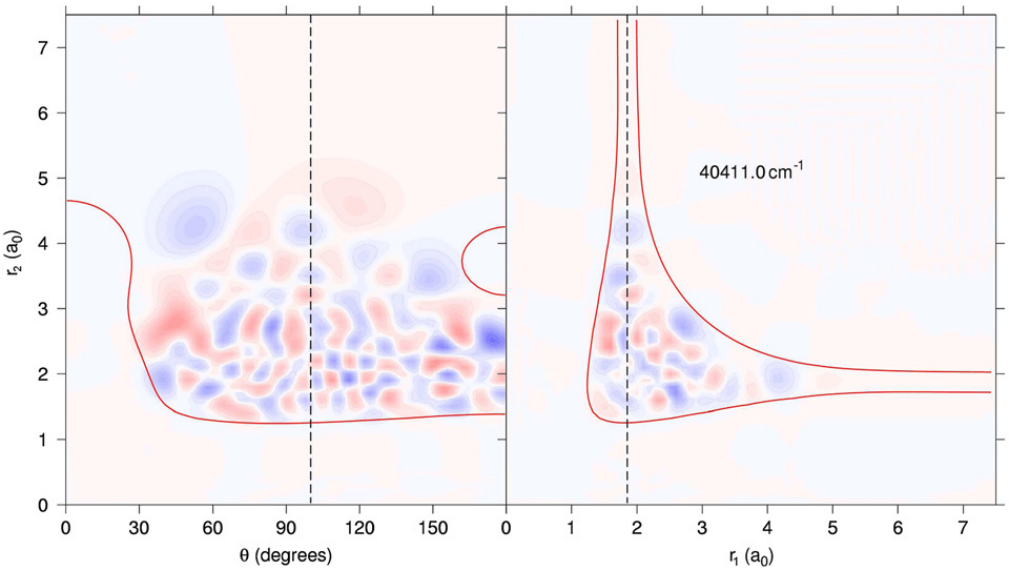

Fig. 5. Wave function plot for an ergodic state. For a detailed description see the legend to Fig. 2.

shows, even when normal mode labels can be allocated based on this scheme, their physical relevance can clearly be questioned.

2. Wave function plots. Inspection of 2D cuts of the real wave function plots along appropriately chosen coordinates sometimes gives valuable qualitative information on the level and is particularly useful for states of more or less pure stretching or bending character. However, plots cannot be used to get quantitative information on mixtures without significant manipulation [72], which was not attempted here. It would also be hard to identify multiply excited levels, e.g., (5 5 5), by visual inspection even if such a state was fairly harmonic.
3. Mean values of squares of the Jensen coordinates $\langle s_i^2 \rangle$ i=1,2,3 [73]. These expectation values were calculated by the program XPECT3 [37]. Normal mode-like labels can be created by rounding the expectation values to the nearest integers. For a harmonic oscillator this label should be proportional to the normal mode quantum number v_i. Indeed, for the lowest-lying levels these labels reproduce the normal mode labels of the most dominant harmonic oscillator functions contributing to the "exact" state. However, for a Morse-like real oscillator the well is wider and the mean values grow quicker than v_i. Thus, $\langle s_i^2 \rangle$ for the two stretching modes grows too fast. The largest 'xpect' stretching quantum numbers are for states (n 0 0), decreasing for other members of the same polyad. The v_2 'xpect' quantum number, on the other hand, grows slower than the "harmonic" quantum number. By extrapolating the behavior of these 'xpect' quantum numbers from states with known labels to unknown ones one can guess normal mode labels. The resulting labels are given in Table 1 under the heading "xpect".
4. Perturbing the bending part of the PES. Assignment of vibrational quantum numbers to levels with large v_2 values is particularly difficult. Therefore, we analyzed the change in the energy of a level with the inclusion of an artificial term in the PES depending only on the angle. For this we actually used a term designed to correct the height of the barrier to linearity of water [60,66,67]. Changes in a level's energy were found to be practically independent of the stretching quantum numbers v_1 and v_3. For values of the bending quantum number v_2 between 0 and 7, shifts in the levels were found to be directly proportional to v_2, greatly facilitating the assignment procedure. Consequently, comparing changes observed for unlabelled levels with those of already labelled ones we could determine the values of v_2 for these states. The maximum change occurred near v_2=8. For higher v_2 values the changes were found to be apparently only indicators that v_2 has a high value.
5. Normal mode decomposition (NMD). Another assignment procedure used in this work was based on the normal mode decomposition [74] of the variational wave function. In the NMD the variationally computed, normalized vibrational wave functions, ψ_i, are characterized by the square of their overlaps with the normalized harmonic oscillator wave functions, ϕ_v^{HO}, expressed in terms of normal coordinates corresponding to the actual PES,

$$\chi_{iv} = |\langle \psi_i | \phi_v^{\mathrm{HO}} \rangle|^2, \tag{2}$$

where v=(v_1 v_2 v_3) is a composite index. For each vibrational state the sum of the NMD entries equals one, $\sum_{j=0} \chi_{ij} = 1$, as the wave function can be expressed as a linear combination of harmonic oscillator wave functions. The wave functions obtained with the DEWE program [47,48] are given in terms of normal coordinates, so the computation of their overlap with the actual harmonic oscillator wave functions is straightforward. As the bending modes of water are very anharmonic and higher bends cannot be treated with the DEWE protocol, the method provides meaningful results only for states with v_2=0 values, as could

Table 1
The lowest 250 vibrational band origins (computed as part of this study and experimental (Expt.)), their symmetries (Sym.), the corresponding polyad number P, defined as $P = 2\nu_1 + \nu_2 + 2\nu_3$, and approximate vibrational assignments corresponding to the PES developed in this paper.[a]

	Energy		Sym.	Approximate assignments				
	ab initio	Expt.		P	Normal	xpect	W_{stre}	Plot
1	1596.37	1594.75	+	1	(0 1 0)	[0 1 0]	–	G
2	3154.45	3151.63	+	2	(0 2 0)	[0 2 0]	–	G
3	3657.41	3657.05	+	2	(1 0 0)	[1 0 0]	0.98	G
4	3755.93	3755.93	–	2	(0 0 1)	[0 0 1]	0.99	G
5	4670.86	4666.79	+	3	(0 3 0)	[0 3 0]	–	G
6	5236.75	5234.97	+	3	(1 1 0)	[1 1 0]	–	G
7	5332.87	5331.27	–	3	(0 1 1)	[0 1 1]	–	G
8	6139.62	6134.01	+	4	(0 4 0)	[0 4 0]	–	G
9	6778.25	6775.09	+	4	(1 2 0)	[1 2 0]	–	G
10	6874.32	6871.52	–	4	(0 2 1)	[0 2 1]	–	G
11	7202.45	7201.54	+	4	(2 0 0)	[2 0 0]	0.96	G
12	7250.44	7249.82	–	4	(1 0 1)	[1 0 1]	0.97	G
13	7444.91	7445.05	+	4	(0 0 2)	[1 0 2]	0.98	G
14	7550.09	7542.44	+	5	(0 5 0)	[0 5 0]	–	G
15	8278.89	8273.98	+	5	(1 3 0)	[1 3 0]	–	G
16	8377.92	8373.85	–	5	(0 3 1)	[0 3 1]	–	G
17	8763.71	8761.58	+	5	(2 1 0)	[2 1 0]	–	G
18	8808.85	8807.00	–	5	(1 1 1)	[1 1 1]	–	G
19	8880.85	8869.95	+	6	(0 6 0)	[0 6 0]	–	G
20	9001.59	9000.14	+	5	(0 1 2)	[1 1 2]	–	G
21	9731.26	9724.3*	+	6	(1 4 0)	[1 4 0]	–	G
22	9839.13	9833.59	–	6	(0 4 1)	[0 4 1]	–	G
23	10 100.36	10 086.05	+	7	(0 7 0)	[0 7 0]	–	G
24	10 287.81	10 284.37	+	6	(2 2 0)	[2 2 1]	–	G
25	10 331.65	10 328.73	–	6	(1 2 1)	[1 2 1]	–	G
26	10 524.53	10 521.76	+	6	(0 2 2)	[1 2 2]	–	G
27	10 600.38	10 599.69	+	6	(3 0 0)	[3 0 1]	0.93	G
28	10 613.82	10 613.35	–	6	(2 0 1)	[2 0 2]	0.94	G
29	10 869.62	10 868.88	+	6	(1 0 2)	[2 0 1]	0.94	G
30	11 032.04	11 032.40	–	6	(0 0 3)	[1 0 3]	0.96	G
31	11 109.00	–	+	7	(1 5 0)	[1 5 0]	–	G
32	11 250.15	11 242.78	–	7	(0 5 1)	[0 5 1]	–	G
33	11 267.44	11 254.00	+	8	(0 8 0)	[0 7 0]	–	G
34	11 772.53	11 767.39	+	7	(2 3 0)	[2 3 1]	–	G
35	11 817.51	11 813.20	–	7	(1 3 1)	[2 3 1]	–	G
36	12 012.03	12 007.78	+	7	(0 3 2)	[1 3 2]	–	G
37	12 140.91	12 139.32	+	7	(3 1 0)	[3 1 2]	–	G
38	12 152.60	12 151.25	–	7	(2 1 1)	[2 1 2]	–	G
39	12 392.96	–	+	8	(1 6 0)	[1 6 0]	–	–

Table 1 (*continued*)

	Energy		Sym.	Approximate assignments				
	ab initio	Expt.		*P*	Normal	xpect	W_{stre}	Plot
40	12 409.80	12 407.66	+	7	(1 1 2)	[2 1 1]	–	G
41	12 545.97	12 533.72	+	9	(0 9 0)	[1 7 0]	–	–
42	12 566.13	12 565.01	–	7	(0 1 3)	[1 1 3]	–	G
43	12 596.07	12 586*	–	8	(0 6 1)	[0 6 1]	–	G
44	13 211.95	13 205.1*	+	8	(2 4 0)	[2 4 0]	–	G
45	13 262.09	13 256.2*	–	8	(1 4 1)	[2 4 1]	–	G
46	13 459.42	13 453.7*	+	8	(0 4 2)	[1 4 2]	–	–
47	13 643.57	13 640.5*	+	8	(3 2 0)	[3 2 2]	–	G
48	13 654.79	13 652.66	–	8	(2 2 1)	[3 2 2]	–	G
49	13 673.82	13 661*	+	9	(1 7 0)	[1 6 0]	–	–
50	13 828.00	13 828.28	+	8	(4 0 0)	[3 0 3]	0.88	G
51	13 830.61	13 830.94	–	8	(3 0 1)	[3 0 3]	0.86	G
52	13 848.43	13 835.37	–	9	(0 7 1)	[1 7 1]	–	G
53	13 869.65	–	+	10	(0 1 0 0)	[1 7 0]	–	G
54	13 914.40	13 910.88	+	8	(1 2 2)	[3 2 1]	–	G
55	14 068.53	14 066.20	–	8	(0 2 3)	[1 2 3]	–	G
56	14 222.08	14 221.16	+	8	(2 0 2)	[4 0 1]	0.90	G
57	14 318.68	14 318.81	–	8	(1 0 3)	[3 0 3]	0.92	G
58	14 536.82	14 537.50	+	8	(0 0 4)	[2 0 4]	0.93	–
59	14 588.61	–	+	9	(2 5 0)	[2 5 0]	–	–
60	14 655.88	14 647.98	–	9	(1 5 1)	[2 5 1]	–	G
61	14 830.83	–	+	9	(0 5 2)	[1 6 1]	–	–
62	14 892.78	–	+	10	(1 8 0)	[1 6 1]	–	G
63	14 999.08	–	–	10	(0 8 1)	[1 7 1]	–	G
64	15 111.86	15 108.24	+	9	(3 3 0)	[3 3 2]	–	G
65	15 122.37	15 119.03	–	9	(2 3 1)	[3 3 2]	–	G
66	15 305.69	–	+	11	(0 1 1 0)	[1 7 0]	–	G
67	15 345.07	15 344.50	+	9	(4 1 0)	[4 1 3]	–	G
68	15 348.16	15 347.96	–	9	(3 1 1)	[4 1 3]	–	G
69	15 382.63	15 377.7*	+	9	(1 3 2)	[3 3 1]	–	G
70	15 538.43	15 534.71	–	9	(0 3 3)	[1 3 3]	–	G
71	15 744.91	15 742.80	+	9	(2 1 2)	[4 1 1]	–	G
72	15 833.74	15 832.78	–	9	(1 1 3)	[3 1 3]	–	–
73	15 882.40	15 871*	+	10	(2 6 0)	[2 6 0]	–	–
74	15 979.45	15 969*	–	10	(1 6 1)	[2 6 1]	–	G
75	16 047.67	16 046*	+	9	(0 1 4)	[2 1 4]	–	G
76	16 085.44	–	+	11	(1 9 0)	[2 7 1]	–	–
77	16 173.80	–	–	11	(0 9 1)	[1 7 1]	–	G
78	16 225.40	16 215*	+	10	(0 6 2)	[1 6 2]	–	G
79	16 539.55	16 534.5*	+	10	(3 4 0)	[3 4 2]	–	G
80	16 551.02	16 546.32	–	10	(2 4 1)	[3 4 2]	–	G
81	16 802.10	16 795.9*	+	10	(1 4 2)	[3 3 2]	–	G
82	16 822.18	16 821.63	–	10	(3 2 1)	[4 2 3]	–	G
83	16 824.94	16 823.32	+	10	(4 2 0)	[4 2 3]	–	G
84	16 833.78	–	+	12	(0 1 2 0)	[1 7 0]	–	G
85	16 897.29	16 898.4*	+	10	(5 0 0)	[4 1 4]	0.68	G
86	16 897.70	16 898.84	–	10	(4 0 1)	[4 1 4]	0.68	G
87	16 972.71	16 967.6*	–	11	(0 4 3)	[2 4 3]	–	G

88	17 151.43		+	11	(270)	[260]	–	G
89	17 230.92		+	10	(222)	[421]	–	G
90	17 242.04	–	–	11	(171)	[261]	–	G
91	17 314.59	17 312.55	–	10	(123)	[323]	–	G
92	17 396.09	–	+	12	(1100)	[171]	–	G
93	17 456.97	–	–	12	(0101)	[171]	–	G
94	17 458.36	17 458.21	+	10	(302)	[502]	0.86	G
95	17 494.79	17 495.53	–	10	(203)	[403]	0.86	G
96	17 504.05	–	+	11	(072)	[172]	–	G
97	17 528.34	17 526.3*	+	10	(024)	[224]	–	G
98	17 748.00	17 748.11	+	10	(104)	[403]	0.88	G
99	17 918.45	17 911.6*	+	11	(350)	[341]	–	G
100	17 934.32	17 928*	–	11	(251)	[342]	–	G
101	17 947.30	–	–	10	(005)	[205]	0.91	G
102	18 170.61	18 162*	+	11	(152)	[351]	–	–
103	18 267.50	18 265.82	–	11	(331)	[433]	–	G
104	18 268.81	18 267.1*	+	11	(430)	[433]	–	G
105	18 346.16	–	+	12	(280)	[270]	–	G
106	18 357.81	18 350.3*	–	11	(053)	[253]	–	–
107	18 391.95	18 392.78	+	11	(510)	[524]	–	G
108	18 392.51	18 393.31	–	11	(411)	[524]	–	G
109	18 435.01	–	+	13	(0130)	[180]	–	G
110	18 436.95	–	–	12	(181)	[272]	–	G
111	18 657.57	–	+	12	(082)	[172]	–	G
112	18 680.15	–	+	11	(232)	[431]	–	G
113	18 761.97	18 758.63	–	11	(133)	[333]	–	G
114	18 817.64	–	+	13	(1110)	[280]	–	G
115	18 830.31	–	–	13	(0111)	[181]	–	G
116	18 957.16	18 955.7*	+	11	(312)	[512]	–	G
117	18 980.19	18 977.2*	+	11	(034)	[334]	–	G
118	18 990.12	18 989.96	–	11	(213)	[413]	–	G
119	19 232.48	19 223.5*	+	12	(360)	[351]	–	G
120	19 243.31	–	+	11	(114)	[413]	–	G
121	19 258.70	19 250*	–	12	(261)	[352]	–	G
122	19 432.72	–	–	11	(015)	[315]	–	G
123	19 451.40	–	+	12	(162)	[362]	–	G
124	19 564.31	–	–	13	(191)	[272]	–	G
125	19 587.41	–	+	13	(290)	[371]	–	G
126	19 680.63	19 677.8*	+	12	(440)	[433]	–	G
127	19 682.08	19 679.19	–	12	(341)	[433]	–	G
128	19 729.44	19 720.2*	–	12	(063)	[253]	–	G
129	19 779.54	19 781.32	+	12	(600)	[605]	0.87	G
130	19 779.78	19 781.10	–	12	(501)	[605]	0.88	G
131	19 793.51	–	+	13	(092)	[182]	–	G
132	19 864.02	19 864.7*	+	12	(520)	[524]	–	G
133	19 864.47	19 865.28	–	12	(421)	[524]	–	G
134	20 039.28	–	+	14	(0140)	[170]	–	G
135	20 085.94	–	+	12	(242)	[541]	–	G
136	20 173.47	–	–	12	(143)	[343]	–	G
137	20 288.91	–	–	14	(0121)	[181]	–	G
138	20 321.93	–	+	14	(1120)	[280]	–	G
139	20 390.73	–	+	12	(044)	[334]	–	G
140	20 421.53	–	+	12	(322)	[522]	–	G

Table 1 (*continued*)

	Energy		Sym.	Approximate assignments				
	ab initio	Expt.		*P*	Normal	xpect	W_{stre}	Plot
141	20 443.66	20 442.78	–	12	(2 2 3)	[5 2 3]	–	G
142	20 502.98	–	+	13	(3 7 0)	[3 6 1]	–	G
143	20 526.34	–	–	13	(2 7 1)	[3 6 2]	–	G
144	20 532.45	20 534.5*	+	12	(4 0 2)	[6 0 4]	0.74	G
145	20 541.96	20 543.13	–	12	(3 0 3)	[6 1 4]	0.70	G
146	20 702.48	–	+	12	(1 2 4)	[4 2 3]	–	G
147	20 731.38	–	+	13	(1 7 2)	[3 6 2]	–	G
148	20 813.03	–	–	14	(1 1 0 1)	[2 8 2]	–	G
149	20 846.69	–	+	14	(2 1 0 0)	[3 7 1]	–	G
150	20 888.28	–	–	12	(0 2 5)	[3 2 5]	–	G
151	20 906.28	–	+	12	(2 0 4)	[6 0 2]	0.82	G
152	21 016.05	–	–	13	(0 7 3)	[2 6 3]	–	G
153	21 016.42	–	+	14	(0 1 0 2)	[2 8 2]	–	G
154	21 040.68	–	–	12	(1 0 5)	[5 0 4]	0.83	G
155	21 056.29	21 052*	+	13	(4 5 0)	[4 4 3]	–	G
156	21 057.74	21 053*	–	13	(3 5 1)	[4 4 3]	–	G
157	21 221.16	21 221.57	+	13	(6 1 0)	[6 2 5]	–	G
158	21 221.48	21 221.83	–	13	(5 1 1)	[6 2 5]	–	G
159	21 272.94	–	+	12	(0 0 6)	[3 0 6]	0.87	G
160	21 312.99	21 312*	+	13	(5 3 0)	[5 3 5]	–	F
161	21 313.69	21 314.45	–	13	(4 3 1)	[5 3 5]	–	G
162	21 438.30	–	+	13	(2 5 2)	[5 5 1]	–	G
163	21 539.81	–	–	13	(1 5 3)	[3 5 3]	–	G
164	21 639.05	–	+	15	(0 1 5 0)	[2 7 0]	–	G
165	21 715.72	–	+	14	(3 8 0)	[3 7 1]	–	G
166	21 720.50	–	–	14	(2 8 1)	[3 7 2]	–	G
167	21 770.36	–	+	13	(0 5 4)	[3 4 4]	–	G
168	21 820.43	–	–	15	(0 1 3 1)	[2 8 1]	–	G
169	21 847.82	–	+	13	(3 3 2)	[5 3 2]	–	G
170	21 869.17	21 867*	–	13	(2 3 3)	[5 3 3]	–	G
171	21 926.33	–	+	15	(1 1 3 0)	[2 8 1]	–	G
172	21 984.51	–	+	14	(1 8 2)	[3 7 1]	–	G
173	22 006.94	–	+	13	(4 1 2)	[6 2 4]	–	G
174	22 014.97	22 015*	–	13	(3 1 3)	[6 2 4]	–	G
175	22 131.40	–	+	13	(1 3 4)	[5 3 3]	–	G
176	22 142.51	–	–	15	(1 1 1 1)	[2 8 2]	–	G
177	22 176.51	–	+	15	(2 1 1 0)	[2 8 1]	–	G
178	22 234.85	–	–	14	(0 8 3)	[2 7 3]	–	G
179	22 315.57	–	–	13	(0 3 5)	[3 3 5]	–	G
180	22 338.62	–	+	15	(0 1 1 2)	[2 8 1]	–	G
181	22 382.53	22 376*	+	14	(4 6 0)	[5 5 3]	–	G
182	22 383.89	22 377*	–	14	(3 6 1)	[4 5 3]	–	G
183	22 387.51	–	+	13	(2 1 4)	[6 2 2]	–	G
184	22 507.61	22 508*	–	13	(1 1 5)	[5 1 4]	–	G
185	22 528.67	22 529.29	+	14	(7 0 0)	[8 0 7]	0.92	G
186	22 528.80	22 529.44	–	14	(6 0 1)	[8 0 7]	0.92	G
187	22 628.47	22 626*	+	14	(6 2 0)	[6 3 5]	–	G

188	22 630.29	22 629*	–	14	(521)	[635]	–	0.00	0.00	G	G
189	22 708.35	–	+	14	(262)	[552]	–	77.35	77.35	G	G
190	22 732.30	–	+	13	(016)	[416]	–	101.30	101.30	G	G
191	22 738.51	–	–	14	(441)	[635]	–	107.51	107.51	G	G
192	22 744.61	–	+	14	(540)	[545]	–	113.61	113.61	G	G
193	22 810.73	–	–	15	(291)	[373]	–	179.73	179.73	G	G
194	22 885.31	–	+	15	(390)	[471]	–	254.31	254.31	G	G
195	22 925.68	–	–	14	(163)	[362]	–	294.68	294.68	–	–
196	23 067.43	–	+	15	(192)	[363]	–	436.43	436.43	–	–
197	23 157.70	–	+	14	(064)	[363]	–	526.70	526.70	–	–
198	23 236.60	–	+	14	(342)	[642]	–	605.60	605.60	G	G
199	23 257.08	–	–	14	(243)	[543]	–	626.08	626.08	G	G
200	23 263.52	–	+	16	(1140)	[370]	–	632.52	632.52	G	G
201	23 322.45	–	–	15	(093)	[283]	–	691.45	691.45	–	–
202	23 366.38	–	–	16	(0141)	[282]	–	735.38	735.38	G	G
203	23 400.04	23 401*	+	14	(502)	[715]	0.74	769.04	769.04	G	G
204	23 404.07	23 405.4*	–	14	(403)	[715]	0.76	773.07	773.07	G	G
205	23 466.78	–	+	14	(422)	[624]	–	835.78	835.78	G	G
206	23 474.45	–	–	14	(323)	[625]	–	843.45	843.45	G	G
207	23 524.78	–	+	14	(144)	[543]	–	893.78	893.78	G	G
208	23 559.74	–	+	16	(2120)	[381]	–	928.74	928.74	G	G
209	23 605.07	–	–	16	(1121)	[382]	–	974.07	974.07	G	G
210	23 652.29	–	+	16	(0160)	[372]	–	1021.29	1021.29	–	–
211	23 663.89	–	+	15	(470)	[372]	–	1032.89	1032.89	–	–
212	23 665.77	–	–	15	(371)	[463]	–	1034.77	1034.77	G	G
213	23 713.51	–	–	14	(045)	[345]	–	1082.51	1082.51	G	G
214	23 787.05	–	+	16	(0122)	[281]	–	1156.05	1156.05	–	–
215	23 825.74	–	+	14	(224)	[722]	–	1194.74	1194.74	G	G
216	23 935.12	23 934*	–	14	(125)	[625]	–	1304.12	1304.12	G	G
217	23 944.48	23 942*	+	15	(710)	[726]	–	1313.48	1313.48	G	G
218	23 947.68	23 947*	–	15	(611)	[717]	–	1316.68	1316.68	G	G
219	23 960.85	–	+	15	(272)	[553]	–	1329.85	1329.85	–	–
220	23 977.25	–	+	14	(304)	[813]	0.73	1346.25	1346.25	G	G
221	23 998.57	–	–	15	(451)	[554]	–	1367.57	1367.57	–	–
222	24 015.44	–	+	15	(550)	[645]	–	1384.44	1384.44	G	G
223	24 033.57	–	–	16	(2101)	[463]	–	1402.57	1402.57	–	–
224	24 038.37	–	–	14	(205)	[714]	0.69	1407.37	1407.37	G	G
225	24 091.22	–	+	16	(3100)	[482]	–	1460.22	1460.22	G	G
226	24 142.76	–	–	15	(531)	[646]	–	1511.76	1511.76	G	G
227	24 143.05	–	+	15	(630)	[646]	–	1512.05	1512.05	F	F
228	24 162.05	–	+	14	(026)	[426]	–	1531.05	1531.05	G	G
229	24 177.98	–	–	15	(173)	[463]	–	1546.98	1546.98	–	–
230	24 290.62	–	+	14	(106)	[605]	0.78	1659.62	1659.62	G	G
231	24 312.65	–	+	16	(1102)	[372]	–	1681.65	1681.65	F	F
232	24 435.42	–	+	15	(074)	[363]	–	1804.42	1804.42	F	F
233	24 466.99	–	–	16	(0103)	[283]	–	1835.99	1835.99	F	F
234	24 508.22	–	–	14	(007)	[407]	0.83	1877.22	1877.22	G	G
235	24 582.36	–	+	15	(352)	[642]	–	1951.36	1951.36	F	F
236	24 609.05	–	–	15	(253)	[543]	–	1978.05	1978.05	G	G
237	24 798.22	–	+	15	(512)	[734]	–	2167.22	2167.22	–	–
238	24 807.86	–	–	15	(413)	[725]	–	2176.86	2176.86	–	–
239	24 826.40	–	+	17	(2130)	[461]	–	2195.40	2195.40	F	F
240	24 856.94	–	–	16	(381)	[463]	–	2225.94	2225.94	–	–
241	24 869.48	–	+	15	(154)	[543]	–	2238.48	2238.48	–	–

Table 1 (*continued*)

	Energy		Sym.	Approximate assignments				
	ab initio	Expt.		*P*	Normal	xpect	W_{stre}	Plot
242	24 883.66	–	+	16	(4 8 0)	[4 7 2]	–	F
243	24 910.71	–	−	15	(3 3 3)	[6 3 4]	–	–
244	24 915.51	–	+	15	(4 3 2)	[6 3 4]	–	–
245	24 925.35	–	−	17	(1 1 3 1)	[3 7 2]	–	F
246	25 077.92	–	−	15	(0 5 5)	[3 4 5]	–	G
247	25 094.22	–	+	17	(1 1 5 0)	[2 8 2]	–	F
248	25 121.48	25 120*	+	16	(8 0 0)	[10 0 10]	0.89	F
249	25 121.50	25 120.28	−	16	(7 0 1)	[10 0 10]	0.89	G
250	25 156.46	–	+	17	(0 1 3 2)	[4 7 1]	–	–

[a] Sym., permutation symmetry characterized also by $(-1)^{v_3}$ for states with a normal mode assignment. Normal, normal mode assignment (v_1 v_2 v_3) based on the normal mode quantum numbers v_1, v_2, and v_3 for the symmetric stretch, bend, and antisymmetric stretch modes. xpect, expectation values of the squares of the Jensen coordinates rounded to the nearest integer (see text). W_{stre}, stretching weight in the wave function, calculated according to Eq. (3). The band centers marked with an asterisk were estimated from levels with $J > 0$. Under "Plot", G, good and F, fair, –, plot does not yield labels.

be seen when comparing the eigenvalues obtained with DVR3D and DEWE (the latter are not presented here).

The mean values of the squares of the Jensen coordinates provide meaningful labels for the lowest vibrational levels. The labels obtained agree with the chosen normal mode labels up to (0 0 2) at 7441.91 cm^{-1}. Above this state there are still a lot of meaningful labels but they increasingly start to break down. Of course, the meaningful labels are the same as those produced by the energy decomposition scheme.

According to the NMD analysis, the lowest-lying vibrational energy levels are characterized by a single, dominant harmonic oscillator function, and thus their assignment is absolutely unambiguous. For example, the vibrational state at 4670.86 cm^{-1} and described as (0 3 0) with a polyad number $P = 3$, where $P = 2v_1 + v_2 + 2v_3$, is the following mixture of the harmonic oscillator basis states: 0.88(0 3 0) + 0.05(1 1 0) + 0.03(0 4 0). At the same time, for higher-lying levels, with polyad numbers $P = 4-6$, i.e., the second and third stretching overtone and combination levels, the identification of a single, dominant harmonic oscillator wave function is not possible. Already for these states the attachment of a single (v_1 v_2 v_3) normal mode label cannot be carried out without overwhelming and steadily increasing ambiguities. For example, it seems completely natural to give the labels (4 0 0) and (2 0 2) to the states computed at 13 828 and 14 222 cm^{-1}. Nevertheless, the NMD analysis clearly indicates that the harmonic oscillator basis functions (4 0 0) and (2 0 2) have basically zero weight in both exact wave functions. Both wave functions are extremely heavy mixtures of the basis states, the largest NMD contributions are 0.20(1 0 2), 0.12(3 0 2), and 0.11(3 0 0) for the state at 13 828 cm^{-1}, and 0.21(5 0 0), 0.18(3 0 0), and 0.11(1 0 2) for the state at 14 222 cm^{-1}. It is of particular interest to note that Choi and Light [75], based on their wave function analysis, reversed the order of the (4 0 0) and (2 0 2) states. The reverse order is supported by the 'xpect' values of this study (Table 1). Nevertheless, due to the indications of the NMD analysis, we decided to keep the original, intuitively appealing ordering.

Thus, it is important to emphasize that the distribution of the possible normal mode labels (v_1 v_2 v_3) is not rooted in firm theory but simply in tradition. Apart from the fundamentals and maybe low-lying overtones and combination levels, the linear combination of the "exact" variational wave function in terms of harmonic oscillator basis functions is typically not dominated by a single harmonic oscillator function. Despite the strong mixing of harmonic oscillator wave functions in excited vibrational levels, we attempted to employ the NMD analysis to justify the distribution of some normal mode labels. The intention was to identify "pure" stretching states, $(v_1\,0\,v_3)v_1, v_3 = 0, 1, \ldots$. In order to do this, the "stretching weight", W_{stre}, and the "number of stretching quanta", N_{stre}, were introduced as

$$W_{stre} = \sum_{v_1,v_3} \chi_{i,v=(v_1,0,v_3)} \tag{3}$$

Table 2
High-energy vibrational states with vibrational quantum number assignments.

No.	$\tilde{\nu}_{\text{theo}}$	par	Label	Plot	W_{stre}	$\tilde{\nu}_{\text{Exp}}$
251	25 157.16	–	(0 15 1)	wfp		
252	25 228.72	+	(2 3 4)			
253	25 265.78	+	(2 8 2)			
254	25 297.29	–	(1 8 3)			
255	25 316.50	+	(5 6 0)			
256	25 322.53	–	(4 6 1)			
257	25 338.88	–	(1 3 5)			
258	25 359.12	+	(3 11 0)	wfp		
259	25 371.53	–	(6 2 1)			
260	25 372.71	+	(7 2 0)	wfp		
261	25 407.13	–	(2 11 1)	wfp		
262	25 436.15	+	(3 1 4)	wfp		
263	25 475.75	+	(0 17 0)	wfp		
264	25 486.84	–	(2 1 5)			
265	25 519.33	+	(6 4 0)	wfp		
266	25 519.70	–	(5 4 1)			
267	25 565.47	+	(0 3 6)	wfp		
268	25 606.61	+	(0 8 4)	wfp		
269	25 689.97	+	(1 11 2)			
270	25 712.28	–	(0 11 3)	wfp		
271	25 735.97	+	(1 1 6)	wfp		
272	25 860.53	+	(3 6 2)	wfp		
273	25 891.48	–	(2 6 3)			
274	25 939.41	–	(0 1 7)			
275	26 033.48	+	(4 9 0)	wfp		
276	26 037.33	–	(3 9 1)	wfp		
277	26 133.81	+	(6 0 2)		0.78	
278	26 141.83	–	(5 0 3)	wfp	0.80	
279	26 150.66	+	(1 6 4)			
280	26 197.10	–	(3 4 3)			
281	26 206.72	+	(4 4 2)			
282	26 321.84	+	(5 2 2)			
283	26 321.92	–	(4 2 3)	ok		
284	26 357.01	+	(2 9 2)	wfp		
285	26 393.20	–	(1 9 3)	wfp		
286	26 428.83	+	(2 14 0)			
287	26 432.58	–	(0 14 1)			
288	26 517.91	+	(8 1 0)	wfp		
290	26 517.96	–	(7 1 1)	wfp		
291	26 598.25	+	(3 12 0)			
292	26 603.02	+	(0 14 2)			
293	26 712.53	–	(2 12 1)			
297	26 736.36	–	(6 3 1)			
299	26 736.43	+	(7 3 0)			
300	26 774.80	+	(0 9 4)			
301	26 825.82	–	(0 16 1)	wfp		
302	26 832.12	+	(4 0 4)		0.47	
303	26 839.27	+	(1 16 0)	wfp		
304	26 866.40	–	(3 0 5)	wfp	0.61	
305	26 906.74	+	(3 2 4)			
308	26 934.53	–	(2 2 5)	wfp		
309	26 942.74	+	(0 4 6)	wfp		
310	27 099.79	–	(0 12 3)			
313	27 105.02	+	(1 12 2)			
314	27 213.93	+	(4 10 0)	wfp		
316	27 243.07	–	(3 10 1)	wfp		
317	27 263.00	+	(2 0 6)	wfp	0.66	
318	27 279.09	+	(0 18 0)	wfp		
319	27 338.95	–	(0 2 7)	wfp		
320	27 422.86	–	(1 0 7)	wfp	0.69	
322	27 499.54	–	(4 3 3)			27 497.2*
323	27 504.57	+	(5 3 2)			27 502.66
324	27 539.87	–	(8 0 1)		0.51	27 536.3*
325	27 544.20	+	(9 0 0)		0.50	27 540.69
326	27 573.10	–	(5 1 3)			27 569.7*
327	27 576.89	+	(6 1 2)			27 574.91
328	27 601.62	–	(1 10 3)			
329	27 603.94	+	(2 10 2)			
330	27 659.15	+	(0 0 8)	wfp	0.79	
331	27 864.31	+	(0 10 4)			

Table 2 (*continued*)

No.	$\tilde{\nu}_{\text{theo}}$	par	Label	Plot	W_{stre}	$\tilde{\nu}_{\text{Exp}}$
337	27 892.06	+	(8 2 0)	wfp		
338	27 892.11	–	(7 2 2)	wfp		
339	27 942.95	+	(2 15 0)	wfp		
341	27 949.51	–	(1 15 1)	wfp		
342	28 072.52	+	(7 4 0)			
344	28 073.18	–	(6 4 1)	wfp		
345	28 107.85	+	(0 15 2)	wfp		
346	28 206.95	+	(3 3 4)			
350	28 243.29	–	(2 3 5)			
352	28 288.20	+	(0 5 6)	wfp		
353	28 337.68	+	(4 1 4)			
356	28 355.33	–	(3 1 5)			
357	28 521.13	+	(1 3 6)	wfp		
362	28 548.19	–	(0 17 1)	wfp		
363	28 629.96	+	(1 17 0)			
364	28 695.77	+	(2 1 6)			
365	28 713.75	–	(0 3 7)			
367	28 719.39	–	(6 0 3)		0.69	
368	28 719.63	+	(7 0 2)		0.74	
369	28 837.71	–	(1 1 7)	wfp		
373	28 893.69	+	(6 2 2)			28 890.1*
375	28 894.10	–	(5 2 3)			28 890.6*
376	28 937.73	+	(9 1 0)	wfp		28 934.14
377	28 938.05	–	(8 1 1)			28 934.4*
378	29 061.60	+	(0 1 8)	wfp		
383	29 107.45	+	(0 19 0)	wfp		
386	29 242.09	–	(7 3 1)	wfp		
388	29 242.09	+	(8 3 0)	wfp		
389	29 372.33	+	(7 5 0)	wfp		
391	29 416.59	+	(2 16 0)			
393	29 418.69	–	(1 16 1)	wfp		
394	29 620.12	+	(5 0 4)		0.51	
403	29 626.92	–	(4 0 5)		0.45	
404	29 707.71	+	(0 16 2)			
406	29 735.62	+	(4 2 4)			
407	29 751.17	–	(3 2 5)			
408	29 817.04	+	(10 0 0)	wfp	0.84	29 810.85
411	29 817.06	–	(9 0 1)	wfp	0.84	29 810.87
412	30 063.49	+	(7 1 2)	wfp		
420	30 069.57	–	(6 1 3)			
421	30 082.30	+	(2 2 6)	wfp		
423	30 170.74	+	(3 0 6)		0.46	
426	30 195.28	–	(2 0 7)	wfp	0.50	
429	30 245.18	+	(6 3 2)			
430	30 246.13	–	(5 3 3)			
431	30 260.15	–	(0 18 1)	wfp		
432	30 282.81	+	(9 2 0)			
434	30 285.03	–	(8 2 1)	wfp		
435	30 314.96	+	(1 18 0)			
436	30 430.56	+	(0 2 8)	wfp		
440	30 501.35	+	(1 0 8)	wfp		
442	30 562.79	+	(8 4 0)			
444	30 562.92	–	(7 4 1)	wfp		
445	30 722.49	–	(0 0 9)	wfp	0.75	
450	30 893.89	+	(3 5 4)			
456	30 964.32	+	(0 20 0)	wfp		
459	30 970.29	+	(5 1 4)			
460	30 979.20	–	(4 1 5)			
461	31 077.13	+	(10 1 0)	wfp		31 071.57
462	31 078.62	–	(9 1 1)	wfp		31 070.7*
463	31 105.59	+	(4 3 4)			
466	31 120.52	–	(3 3 5)			
467	31 161.54	+	(2 17 0)			
468	31 211.96	+	(8 0 2)	wfp	0.6	31 207.09
472	31 212.02	–	(7 0 3)	wfp	0.6	31 212.3*
473	31 287.70	–	(1 17 1)			
475	31 386.89	+	(7 2 2)			
478	31 392.14	–	(6 2 3)			
480	31 510.67	+	(0 17 2)			
484	31 585.29	+	(3 1 6)			
488	31 607.48	+	(9 3 0)			

Table 2 (*continued*)

No.	$\tilde{\nu}_{\text{theo}}$	par	Label	Plot	W_{stre}	$\tilde{\nu}_{\text{Exp}}$
490	31 607.88	–	(8 3 1)	wfp		
491	31 654.75	–	(2 1 7)			
494	31 778.63	+	(0 3 8)	wfp		
498	31 892.22	+	(1 1 8)			
504	31 917.22	–	(10 0 1)	wfp	0.81	31 905.3*
506	31 917.23	+	(11 0 0)	wfp	0.81	31 909.68
507	31 996.00	–	(0 19 1)	wfp		
509	32 094.02	–	(0 1 9)	wfp		
513	32 160.43	–	(5 0 5)		0.68	
515	32 169.87	+	(6 0 4)	wfp	0.37	
516	32 190.74	+	(1 19 0)	wfp		
519	32 298.84	+	(5 2 4)			
523	32 361.87	+	(10 2 0)	wfp		
525	32 364.45	–	(9 2 1)	wfp		
526	32 564.47	+	(8 1 2)			
534	32 564.56	–	(7 1 3)			
535	32 676.74	–	(6 3 3)			
538	32 677.03	+	(7 3 2)			
539	32 832.36	+	(0 21 0)	wfp		
547	32 884.73	+	(4 0 6)		0.69	
549	32 903.53	+	(9 4 0)			
551	32 922.45	–	(3 0 7)	wfp	0.55	
554	32 927.07	–	(9 4 1)	wfp		
556	33 102.82	+	(0 4 8)	wfp		
563	33 152.66	+	(11 1 0)	wfp		33 144.71
566	33 152.70	–	(10 1 1)	wfp		33 144.7*
567	33 182.07	+	(2 18 0)	wfp		
570	33 228.07	+	(2 0 8)		0.43	
571	33 249.83	–	(1 18 1)	wfp		
572	33 421.02	–	(0 2 9)			
580	33 427.19	+	(9 0 2)	wfp	0.69	
581	33 428.88	–	(8 0 3)		0.63	
582	33 476.08	–	(1 0 9)		0.37	
584	33 488.04	+	(6 1 4)			
585	33 489.77	–	(5 1 5)			
586	33 533.51	+	(0 18 2)			
587	33 621.49	–	(9 3 1)			
591	33 629.32	+	(10 3 0)	wfp		
592	33 702.68	+	(0 0 10)	wfp	0.71	
597	33 757.10	–	(0 20 1)	wfp		
598	33 842.41	–	(11 0 1)	wfp	0.78	33 835.22
601	33 842.42	+	(12 0 0)	wfp	0.78	33 835.25
602	33 891.54	+	(8 2 2)	wfp		
605	33 891.64	–	(7 2 3)	wfp		
606	33 973.74	+	(1 20 0)	wfp		
613	34 344.87	+	(4 1 6)			
630	34 368.60	–	(10 2 1)	wfp		
631	34 368.94	+	(11 2 0)	wfp		
632	34 572.39	–	(6 0 5)		0.61	
645	34 572.74	+	(7 0 4)	wfp	0.58	
646	34 676.53	+	(0 22 0)	wfp		
649	34 687.36	+	(2 1 8)	wfp		
650	34 735.04	+	(7 2 4)			
652	34 832.01	–	(1 1 9)	wfp		
660	35 025.35	–	(11 1 1)	wfp		
670	35 025.36	+	(12 1 0)	wfp		
671	35 043.00	+	(0 1 10)	wfp		
672	35 055.57	+	(10 4 0)			
673	35 448.85	+	(5 0 6)		0.44	
693	35 460.76	–	(4 0 7)		0.63	
695	35 515.62	+	(10 0 2)		0.79	35 507*
698	35 516.88	–	(9 0 3)	wfp	0.79	35 509.68
699	35 519.58	–	(0 21 1)	wfp		
700	35 555.90	–	(11 0 3)			
704	35 562.73	+	(11 3 0)	wfp		35 554*
705	35 591.84	+	(13 0 0)	wfp	0.68	35 585.96
709	35 592.40	–	(12 1 0)	wfp	0.66	35 586.01
710	35 836.28	+	(1 21 0)	wfp		
721	35 851.89	–	(8 2 3)	wfp		
723	35 857.44	+	(9 2 2)			
724	35 972.24	+	(3 0 8)	wfp	0.52	
727	36 030.54	–	(0 4 9)	wfp		

Table 2 (*continued*)

No.	$\tilde{\nu}_{\text{theo}}$	par	Label	Plot	W_{stre}	$\tilde{\nu}_{\text{Exp}}$
733	36 093.53	–	(2 0 9)		0.46	
740	36 185.49	+	(12 2 0)	wfp		36 179.32
746	36 185.89	–	(11 2 1)			36 179*
747	36 334.69	+	(1 0 10)	wfp	0.45	
753	36 388.85	+	(0 2 10)			
756	36 597.17	–	(0 0 11)	wfp	0.66	
772	36 687.96	+	(13 1 0)	wfp		36 684.05
776	36 688.90	–	(12 1 1)	wfp		36 684.88
777	36 739.03	+	(0 23 0)	wfp		
780	36 745.30	–	(9 1 3)			36 739.78
782	36 745.63	+	(10 1 2)	wfp		36 740.6
783	36 915.67	+	(8 0 4)		0.36	
795	36 919.29	–	(7 0 5)		0.46	
796	37 122.21	–	(13 0 1)	wfp	0.71	37 122.72
807	37 122.24	+	(14 0 0)	wfp	0.70	37 122.7
808	37 256.54	–	(0 22 1)	wfp		
815	37 312.63	–	(11 3 1)	wfp		37 309.85
821	37 314.57	+	(12 3 0)	wfp		37 311.28
822	37 437.55	–	(12 0 1)		0.73	
832	37 437.55	+	(11 0 2)	wfp	0.72	
833	37 717.05	+	(0 1 11)	wfp		
851	37 742.45	+	(1 22 0)	wfp		
854	37 767.33	–	(12 2 1)	wfp		37 765*
855	37 767.33	+	(13 2 0)	wfp		37 765.65
856	37 824.75	+	(6 0 6)		0.39	
861	37 826.13	–	(5 0 7)		0.25	
862	37 904.14	–	(0 1 11)	wfp		
867	38 149.89	+	(14 1 0)	wfp		38 153.25
883	38 149.94	–	(13 1 1)	wfp		38 153.31
884	38 214.65	+	(8 1 4)			
887	38 219.07	–	(7 1 5)			
888	38 453.59	–	(14 0 1)	wfp	0.69	38 462.54
905	38 453.60	+	(15 0 0)	wfp	0.69	38 462.52
906	38 534.79	+	(4 0 8)	wfp	0.25	
911	38 882.06	+	(0 4 10)	wfp		
940	38 937.90	–	(0 23 1)	wfp		
944	39 118.55	–	(13 2 1)	wfp		39 123*
961	39 118.57	+	(14 2 0)	wfp		39 123.77
962	39 145.48	–	(1 0 11)	wfp	0.34	
963	39 176.43	+	(12 0 2)		0.34	
966	39 176.99	–	(11 0 3)	wfp	0.40	
967	39 375.61	–	(14 1 1)	wfp		39 390.22
986	39 375.61	+	(15 1 0)	wfp		39 390.26
987	39 409.71	+	(0 0 12)	wfp	0.62	
988	39 553.99	+	(16 0 0)	wfp		39 574.54
1001	39 554.01	–	(15 0 1)	wfp		
1002	39 722.21	+	(1 23 0)			
1012	40 022.79	–	(11 1 3)			40 044.72
1037	40 022.81	+	(12 1 2)			40 044.57
1038	40 211.83	+	(15 2 0)	wfp		40 225*
1057	40 212.26	–	(14 2 1)	wfp		40 226.31
1058	40 256.54	–	(13 3 1)			
1061	40 342.35	+	(16 1 0)	wfp		40 370.55
1071	40 342.68	–	(15 1 1)	wfp		40 370.83
1072	40 405.24	+	(17 0 0)	wfp		40 437.23
1080	40 405.40	–	(16 0 1)	wfp		40 437.26
1081	40 698.03	–	(12 0 3)			
1106	40 698.10	+	(13 0 2)			
1107	40 887.34	–	(17 0 1)			
1125	40 889.03	+	(18 0 0)			
1126	40 959.15	–	(16 1 1)			
1132	40 960.40	+	(17 1 0)			
1133	41 055.83	–	(15 2 1)			
1145	41 056.27	+	(16 2 0)			
1146	41 082.75	+	(19 0 0)			
1149	41 082.78	–	(18 0 1)			

A complete set of vibrational levels is given in the supplementary material. wfp, labelling supported by wave function plot. Label, normal mode assignment (ν_1 ν_2 ν_3) based on the normal mode quantum numbers ν_1, ν_2, and ν_3 for the symmetric stretch, bend, and antisymmetric stretch modes. W_{stre}, stretching weight in the wave function, calculated according to Eq. (3). The experimental band centers, $\tilde{\nu}_{\text{Exp}}$, marked with an asterisk were estimated from levels with $J > 0$.

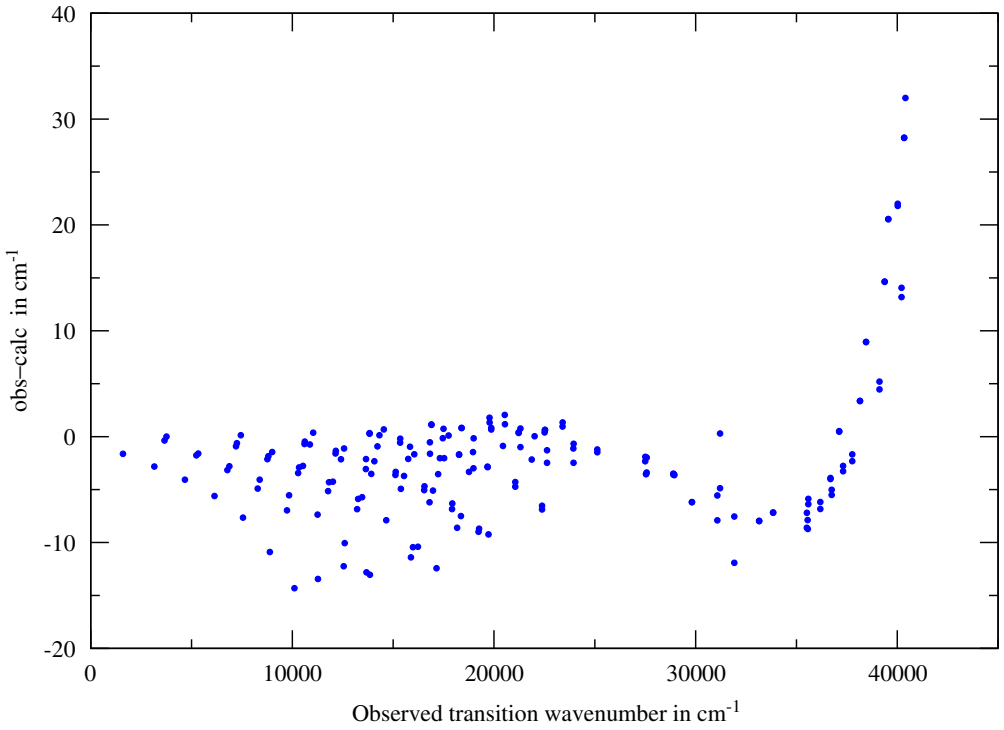

Fig. 6. Differences between the measured and the computed vibrational energy levels utilizing the PES of this study.

and

$$N_{\mathrm{stre}} = \sum_{v_1,v_3} (v_1 + v_3)\chi_{i,v=(v_1,0,v_3)}. \quad (4)$$

In the case of $W_{\mathrm{stre}} > 0.6$, the level was assigned to be a "pure" stretching state. The remaining $1 - W_{\mathrm{stre}}$ contribution is due to harmonic oscillator basis functions in which mixed bending and stretching basis functions or pure bending ones are excited.

Interestingly, above 7445 cm^{-1} N_{stre} did not turn out to be a quantitative measure for the number of exciting quanta on the strictly stretching degrees of freedom (similarly to the Jensen-type 'xpect' values). Furthermore, above 25 000 cm^{-1} certain levels with $0.3 < W_{\mathrm{stre}} < 0.6$ had to be accepted as "pure" stretching states in order to obtain a logically complete labelling. These quantitative defects apart, regularities can be observed in the values of W_{stre} and N_{stre}. Most importantly, the lowest- and highest-lying stretching levels in a polyad have the largest stretching weight, W_{stre}, and the largest number of stretching quanta, N_{stre}.

Table 1 gives vibrational labels for VBOs below 25 200 cm^{-1}. When all the available different procedures agree in the labels, such assignments are considered to be secure. Above 26 500 cm^{-1} the proportion of labelled VBOs, apart from the "pure" stretching VBOs which are labelled up to about 35 000 cm^{-1} with W_{stre} and N_{stre}, drops steadily with energy (Table 2). It may well be possible to assign further labels to these high-lying states but it also true that for these states, apart from isolated cases, visual inspection of each wave function plot yields little insight into the nature of the state.

The following can be observed about the excited pure stretching states. Similarly to many other "trends" observed in the spectroscopy of water, due to the occasional and unpredictable occurrence of resonances these observed "trends" break down. One such trend is the steady alteration of + and − symmetry labels in the sequence of pure stretching states. According to the present PES the first breakdown happens at around 27 540 cm^{-1}, where the (8 0 1) state has a lower energy than the (9 0 0) state. The trend of the formation of more and more close-lying + and − states, such as $(n,0)^{+}0$ and $(n,0)^{-}0$ in local-mode notation, also breaks down. The steady, exponential-like decrease in the computed differences between the $(n,0)^{-}0$ and $(n,0)^{+}0$ energy levels, all in cm^{-1}, 98.52 (P=2), 47.99 (P=4), 13.44 (P=6), 2.61 (P=8), 0.41 (P=10), 0.24 (P=12), 0.13 (P=14), and 0.02 (P=16), jumps to −4.34 for P=18, while it is back to 0.01 for P=20. The same can be said about the state pairs $(n,1)^{+}0$ and $(n,1)^{-}0$, $(n,2)^{+}0$ and $(n,2)^{-}0$, etc., all in local-mode notation. Pure stretching states which correspond to different polyad numbers are in different ranges up to about 27 500 cm^{-1}, where it happens that the first pure stretching member of the P=18 polyad, the by now celebrated (8 0 1) state at 27 539.86 cm^{-1}, has a lower energy than the last pure stretching member of the P=16 polyad occurring at 27 659.15 cm^{-1}. As one moves up in energy, increasing overlap of the polyads is observed.

Despite the drop in the number of assigned VBOs with energy, we are still able to label local mode pairs of the form $(n,0)^{\pm}v_2$ for low values of v_2 all the way to dissociation. Many of these were observed in a recent experimental study [17]. This suggests that our new potential is actually qualitatively different in the near dissociation region to those used in the previous studies which did not appear to support this systematic series of states [3].

4. Conclusions

The following are the main conclusions that can be drawn based on the present computational study:

1. Based principally on 2200 energy points computed at the all-electron, aug-cc-pCV6Z IC-MRCI(8,2) level of electronic structure theory, a new global, mass-independent potential energy surface has been determined for the ground electronic state of the water molecule. The energy points were corrected for relativistic effects via one-electron mass-velocity and Darwin corrections obtained at the same level of theory and in the same calculation. The energy points were fitted to a suitable analytic form allowing for a good global description of the PES toward the first dissociation limit. The PES thus obtained supports 1 150 vibrational energy levels below an energy cutoff value of 41 083 cm^{-1}. The average deviation between the computed and the limited number of experimentally measured energy levels is surprisingly small. Even the maximum deviation is less than 15 cm^{-1} for all the states with energies below 39 500 cm^{-1} (see Fig. 6). Therefore, the use of the present *ab initio* PES for global studies of water is recommended. It is expected that this surface will provide excellent results for the resonance states of water allowing their improved characterization.
2. The following can be said about the virtues and weaknesses of the five wave function assignation protocols analyzed. The simple energy decomposition scheme is rather weak, it can be used only for the lowest eigenstates, and it does not provide labels for all but the simplest cases, which can be investigated by other means, as well. Wave function plots, independent of the actual basis representation but dependent upon the coordinate choice, are highly useful and they are able to provide labels based on node counting. This is particularly true for localized high-energy states where all the energy is in a single mode, see Figs. 1–3 for examples. While for many highly excited states such node counting becomes impossible (see, e.g., Fig. 5), for several states the plots provide information not obtainable by other means. One example is the identification of the highly excited bending state (0 22 0), see Fig. 3. The NMD analysis, though basis and coordinate representation dependent, and the corresponding "stretching weight" as well as the mean values of the squares of the Jensen coordinates provide useful and quantitative measures about the composition of the wave functions. Unfortunately, these measures are also incomplete, break down, or just simply indicate the exceedingly complex character of the wave functions at higher excitations.
3. The distribution of approximate labels referring to normal mode quantum numbers becomes ambiguous above about 26 500 cm^{-1} for all but a few selected states having low or no bending excitation or of pure bends. This is due to the fact that the exact vibrational wave functions become strong mixtures of several basis states.
4. More work is required to obtain completely smooth representations of the dipole moment surface which would allow the wavefunctions given here to be used to estimate vibrational band intensities for states of water lying in the ultraviolet.

Acknowledgements

The Scientific Research Fund of Hungary (Grant OTKA K72885), the European Union QUASAAR Marie Curie research training network, the UK NERC, and the Russian Fund for Basic Research are thanked for their support for aspects of this project. This work was performed as part of the Task Group of the International Union of Pure and Applied Chemistry (IUPAC, Project no. 2004-035-1-100) on "A database of water transitions from experiment and theory".

Appendix A. Supplementary data

Supplementary data associated with this article can be found in the online version at doi:10.1016/j.jqsrt.2010.02.009.

References

[1] Bernath PF. The spectroscopy of water vapour: experiment, theory and applications. Phys Chem Chem Phys 2002;4:1501–9.
[2] Tennyson J, Bernath PF, Brown LR, Campargue A, Carleer MR, Császár AG, et al. Critical evaluation of the rotational–vibrational spectra of water vapor. Part I. Energy levels and transition wavenumbers for H_2 ^{17}O and H_2 ^{18}O. J Quant Spectrosc Radiat Transf 2009;110:573–96.
[3] Mussa HY, Tennyson J. Calculation of rotation–vibration states of water at dissociation. J Chem Phys 1998;109:10885–92.
[4] Gray SK, Goldfield EM. Highly excited bound and low-lying resonance states of H_2O. J Phys Chem 2001;105:2634–41.
[5] Li GH, Guo H. The vibrational level spectrum of H_2O ($X\,^1A'$) from the Partridge–Schwenke potential up to the dissociation limit. J Mol Spectrosc 2001;210:90–7.
[6] Partridge H, Schwenke DW. The determination of an accurate isotope dependent potential energy surface for water from extensive ab initio calculations and experimental data. J Chem Phys 1997;106:4618–39.
[7] Polyansky OL, Császár AG, Shirin SV, Zobov NF, Barletta P, Tennyson J, et al. High accuracy ab initio rotation–vibration transitions of water. Science 2003;299:539–42.
[8] Barletta P, Shirin SV, Zobov NF, Polyansky OL, Tennyson J, Valeev EF, et al. CVRQD adiabatic *ab initio* ground-state potential surfaces for the water molecule. J Chem Phys 2006;125:204307.
[9] Shirin SV, Polyansky OL, Zobov NF, Barletta P, Tennyson J. Spectroscopically determined potential energy surface of H_2 ^{16}O up to 25 000 cm^{-1}. J Chem Phys 2003;118:2124–9.
[10] Shirin SV, Zobov NF, Polyansky OL, Tennyson J, Parekunnel T, Bernath PF. Analysis of hot D_2O emission using spectroscopically-determined potentials. J Chem Phys 2004;120:206–10.
[11] Shirin SV, Polyansky OL, Zobov NF, Ovsyannikov RI, Császár AG, Tennyson J. Spectroscopically determined potential energy surfaces of the H_2 ^{16}O, H_2 ^{17}O and H_2 ^{18}O isotopologues of water. J Molec Spectrosc 2006;236:216–23.
[12] Shirin SV, Zobov NF, Ovsannikov RI, Polyansky OL, Tennyson J. Water line lists close to experimental accuracy using a spectroscopically determined potential energy surface for H_2 ^{16}O, H_2 ^{17}O and H_2 ^{17}O. J Chem Phys 2008;128:224306.
[13] Zobov NF, Belmiloud D, Polyansky OL, Tennyson J, Shirin SV, Carleer M, et al. The near ultraviolet rotation-vibration spectrum of water. J Chem Phys 2000;113:1546–52.

[14] Dupre P, Germain T, Zobov N, Tolchenov R, Tennyson J. Continuous Wave–Cavity ring down near ultraviolet rotation–vibration spectrum of water. J Chem Phys 2005;123:154307.

[15] Callegari A, Theule P, Tolchenov RN, Zobov NF, Polyansky OL, Tennyson J, et al. Dipole moments of highly vibrationally excited water. Science 2002;297:993–5.

[16] Grechko M, Maksyutenko P, Zobov NF, Shirin SV, Polyansky OL, Rizzo TR, et al. Collisionally assisted spectroscopy of water from 27 000 to 34 000 cm^{-1}. J Phys Chem A 2008;112:10539–45.

[17] Grechko M, Boyarkin OV, Rizzo TR, Maksyutenko P, Zobov NF, Shirin S, et al. State-selective spectroscopy of water up to its first dissociation limit. J Chem Phys 2009;131:221105.

[18] Maksyutenko P, Muenter JS, Zobov NF, Shirin SV, Polyansky OL, Rizzo TR, et al. Approaching the full set of energy levels of water. J Chem Phys 2007;126:241101.

[19] Maksyutenko P, Rizzo TR, Boyarkin OV. A direct measurement of the dissociation energy of water. J Chem Phys 2006;125:181101.

[20] Barber RJ, Miller S, Dello Russo N, Mumma MJ, Tennyson J, Guio P. Water in the near IR spectrum of comet 8P/Tuttle. Mon Not R Astron Soc 2009;398:1593–600.

[21] Dunning Jr. TH. Gaussian basis sets for use in correlated molecular calculations. I. The atoms boron through neon and hydrogen. J Chem Phys 1989;90:1007–23.

[22] Wilson AK, van Mourik T, Dunning Jr. TH. Gaussian basis sets for use in correlated molecular calculations. VI. Sextuple zeta correlation consistent basis sets for boron through neon. J Mol Struct (THEOCHEM) 1996;388:339–49.

[23] van Mourik T, Wilson AK, Dunning Jr. TH. Benchmark calculations with correlated molecular wavefunctions. xiii. Potential energy curves for he_2, ne_2, and ar_2 using correlation consistent basis sets through augmented sextuple zeta. Mol Phys 1999;99:529–47.

[24] Wilson AK, Dunning Jr TH. See EMSL basis set exchange web site at ⟨http://bse.pnl.gov/bse/portal⟩; 2008.

[25] Császár AG, Allen WD, Yamaguchi Y, Schaefer III HF. Ab initio determination of accurate potential energy hypersurfaces for the ground electronic states of molecules. In: Jensen P, Bunker PR, editors. Computational molecular spectroscopy. New York: Wiley; 2000.

[26] Császár AG, Allen WD, Schaefer III HF. In pursuit of the *ab initio* limit for conformational energy prototypes. J Chem Phys 1998;108:9751–64.

[27] Werner H-J, Knowles PJ. An efficient internally contracted multiconfiguration-reference configuration interaction method. J Chem Phys 1988;89:5803–14.

[28] Langhoff S, Davidson ER. Size consistency in the dilute helium gas electronic structure. Chem Phys Lett 1977;52:403–6.

[29] Davidson ER, Silver DW. Configuration interaction calculations on the nitrogen molecule. Int J Quant Chem 1974;8:61–72.

[30] Werner H-J, Knowles PJ, Lindh R, Manby FR, Schütz M, et al. Molpro, version 2008.1, a package of ab initio programs, see ⟨www.molpro.net⟩; 2008.

[31] Kállay M, Surján PR. Higher excitations in coupled-cluster theory. J Chem Phys 2001;115:2945–54 for the latest version of the MRCC code see ⟨http://www.mrcc.hu⟩.

[32] Lodi L, Tolchenov RN, Tennyson J, Lynas-Gray AE, Shirin SV, Zobov NF, et al. A high accuracy dipole surface for water. J Chem Phys 2008;128:044304.

[33] Cowan RD, Griffin DC. Approximate relativistic corrections to atomic radial wavefunctions. J Opt Soc Am 1976;66:1010–4.

[34] Tarczay G, Császár AG, Klopper W, Quiney HM. Anatomy of relativistic energy corrections in light molecular systems. Mol Phys 2001;99:1769–94.

[35] Lodi L, Polyansky OL, Tennyson J. On the treatment of long-range interactions in global potential energy surfaces for chemically-bound systems. Mol Phys 2008;106:1267–73.

[36] Henderson JR, Le Sueur CR, Tennyson J. Dvr3d: programs for fully pointwise calculation of vibrational spectra. Comput Phys Commun 1993;75:379–95.

[37] Tennyson J, Kostin MA, Barletta P, Harris GJ, Polyansky OL, Ramanlal J, et al. DVR3D: a program suite for the calculation of rotation–vibration spectra of triatomic molecules. Comput Phys Commun 2004;163:85–116.

[38] Harris DO, Engerholm GG, Gwinn WD. Calculation of matrix elements for one-dimensional quantum-mechanical problems and the application to anharmonic oscillators. J Chem Phys 1965;43:1515–7.

[39] Light JC, Hamilton IP, Lill JV. Generalized discrete variable approximation in quantum mechanics. J Chem Phys 1985;82:1400–9.

[40] Tennyson J, Sutcliffe BT. Variationally exact ro-vibrational levels of the floppy CH_2^+ molecule. J Mol Spectrosc 1983;101:71–82.

[41] Czakó G, Furtenbacher T, Császár AG, Szalay V. Variational vibrational calculations using high-order anharmonic force fields. Mol Phys 2004;102:2411–23.

[42] Szidarovszky T, Czakó G, Császár AG. On the efficiency of treating singularities in triatomic variational vibrational computations. The vibrational states of H_3^+ up to dissociation. J. Chem. Phys., 2010, in press.

[43] Le Sueur CR, Miller S, Tennyson J, Sutcliffe BT. On the use of variational wavefunctions in calculating vibrational band intensities. Mol Phys 1992;76:1147–56.

[44] Schermaul R, Learner RCM, Newnham DA, Ballard J, Zobov NF, Belmiloud D, et al. The water vapour spectrum in the region 8600–15 000 cm^{-1}: experimental and theoretical studies for a new spectral line database ii: Construction and validation. J Molec Spectrosc 2001;208:43–50.

[45] Schwenke DW, Partridge H. Convergence testing of the analytic representation of an ab initio dipole moment function for water: improved fitting yields improved intensities. J Chem Phys 2000;113:6592–7.

[46] Gabriel W, Reinsch E-A, Rosmus P, Carter S, Handy NC. Theoretical integrated vibrational band intensities of water vapor. J Chem Phys 1993;99:897–900.

[47] Mátyus E, Czakó G, Sutcliffe BT, Császár AG. Variational vibrational calculations with arbitrary potentials using the Eckart–Watson Hamiltonians and the discrete variable representation. J Chem Phys 2007;127:084102.

[48] Mátyus E, Simunek J, Császár AG. On variational computation of a large number of vibrational energy levels and wave functions for medium-sized molecules. J Chem Phys 2009;131:074106.

[49] Eckart C. Some studies concerning rotating axes and polyatomic molecules. Phys Rev 1935;47:552–8.

[50] Watson JKG. Simplification of the molecular vibration–rotation Hamiltonian. Mol Phys 1968;15:479–90.

[51] Munro JJ, Silva BC, Tennyson J. Unpublished work, 2009.

[52] Farantos SC, Tennyson J. Quantum and classical vibrational chaos in floppy molecules. J Chem Phys 1985;82:800–9.

[53] Munro JJ, Ramanlal J, Tennyson J. Asymptotic vibrational states of the H_3^+ molecular ion. New J Phys 2005;7:196.

[54] Tennyson J, Zobov NF, Williamson R, Polyansky OL, Bernath PF. Experimental energy levels of the water molecule. J Phys Chem Ref Data 2001;30:735–831.

[55] Zobov NF, Shirin SV, Ovsannikov RI, Polyansky OL, Barber RJ, Tennyson J, et al. Spectrum of hot water in the 4750–13 000 cm^{-1} frequency range. Mon Not R Astron Soc 2008;387:1093–8.

[56] Allen WD, East ALL, Császár AG. Ab initio anharmonic vibrational analyses of non-rigid molecules. In: Laane J, Dakkouri M, van der Veken B, Oberhammer H, editors. Structures and conformations of non-rigid molecules. Dordrecht: Kluwer; 1993. p. 343–73.

[57] Császár AG, Tarczay G, Leininger ML, Polyansky OL, Tennyson J, Allen WD. Dream or reality: complete basis set full configuration interaction potential energy hypersurfaces. In: Demaison J, Sarka K, Cohen EA, editors. Spectroscopy from space, NATO ASI series C. Dordrecht: Kluwer; 2001. p. 317–39.

[58] van Mourik T, Harris GJ, Polyansky OL, Tennyson J, Császár AG, Knowles PJ. *Ab initio* global potential, dipole, adiabatic and relativistic correction surfaces for the HCN/HNC system. J Chem Phys 2001;115:3706–18.

[59] Tarczay G, Császár AG, Klopper W, Szalay V, Allen WD, Schaefer III HF. The barrier to linearity of water. J Chem Phys 1999;110:11971–81.

[60] Valeev EF, Allen WD, Schaefer HF, Császár AG. The second-order Moller–Plesset limit for the barrier to linearity of water. J Chem Phys 2001;114:2875–8.

[61] Császár AG, Czako G, Furtenbacher T, Tennyson J, Szalay V, Shirin SV, et al. On equilibrium structures of the water molecule. J Chem Phys 2005;122:214205.

[62] Ruscic B, Wagner AF, Harding LB, Asher RL, Feller D, Dixon DA, et al. On the enthalpy of formation of hydroxyl radical and gas-phase bond dissociation energies of water and hydroxyl. J Phys Chem 2002;106:2727–47.

[63] Tasi G, Császár AG. Hartree–Fock-limit energies and structures with a few dozen distributed Gaussians. Chem Phys Lett 2007;438:139–43.

[64] Quiney HM, Barletta P, Tarczay G, Császár AG, Polyansky OL, Tennyson J. Two-electron relativistic corrections to the potential energy surface and vibration–rotation levels of water. Chem Phys Lett 2001;344:413–20.

[65] Pyykkö P, Dyall KG, Császár AG, Tarczay G, Polyansky OL, Tennyson J. Lamb shift effects in rotation–vibration spectra of water. Phys Rev A 2001;63:024502.
[66] Császár AG, Kain JS, Polyansky OL, Zobov NF, Tennyson J. Relativistic correction to the potential energy surface and vibration–rotation levels of water. Chem Phys Letts 1998;293:317–23 (erratum 1999;312:613–6).
[67] Kain JS, Polyansky OL, Tennyson J. The ground state potential energy surface of water: barrier to linearity and its effect on the vibration-rotation levels. Chem Phys Lett 2000;317:365–71.
[68] Polyansky OL, Zobov NF, Viti S, Tennyson J, Bernath PF, Wallace L. K band spectrum of water in sunspots. Astrophys J 1997;489: L205–8.
[69] Hose G, Taylor HS. A quantum analog to the classical quasiperiodic motion. J Chem Phys 1982;76:5356–64.
[70] Zobov NF, Ovsyannikov RI, Shirin SV, Polyansky OL. The assignment of quantum numbers in the theoretical spectra of H_2 ^{16}O, H_2 ^{17}O, and H_2 ^{18}O molecules calculated by variational methods in the region 0–26 000 cm^{-1}. Opt Spectrosc 2007;102:348–53.
[71] Carleer M, Jenouvrier A, Vandaele A-C, Bernath PF, Marienne MF, Colin R, et al. The near infrared, visible and near ultraviolet overtone spectrum of water. J Chem Phys 1999;111:2444–50.
[72] Sadovskii DA, Fulton NG, Henderson JR, Tennyson J, Zhilinskii BI. Nonlinear normal modes and local bending vibrations of H_3^+ and D_3^+. J Chem Phys 1993;99:906–18.
[73] Jensen P. The potential-energy surface for the electronic ground-state of the water molecule determined from experimental data using a variational approach. J Mol Spectrosc 1989;133:438–60.
[74] Mátyus E, Fábri C, Szidarovszky T, Czakó G, Allen WD, Asászár AG. Assigning quantum labels to variationally computed rotational-vibrational eigenstates. J. Chem. Phys., 2010, in press.
[75] Choi SE, Light JC. Highly excited vibrational eigenstates of nonlinear triatomic molecules. Application to H_2O. J Chem Phys 1992;97: 7031–54.